

# A20 promotes metastasis of aggressive basal-like breast cancers through multi-monoubiquitylation of Snail1

Ji-Hyung Lee<sup>1,7</sup>, Su Myung Jung<sup>1,7</sup>, Kyung-Min Yang<sup>2</sup>, Eunjin Bae<sup>2</sup>, Sung Gwe Ahn<sup>3</sup>, Jin Seok Park<sup>1</sup>, Dongyeob Seo<sup>1</sup>, Minbeom Kim<sup>1</sup>, Jihoon Ha<sup>1</sup>, Jaewon Lee<sup>1</sup>, Jun-Hyeong Kim<sup>1</sup>, Jun Hwan Kim<sup>1</sup>, Akira Ooshima<sup>2</sup>, Jinah Park<sup>2</sup>, Donghyuk Shin<sup>1</sup>, Youn Sook Lee<sup>1</sup>, Sangho Lee<sup>1</sup>, Geert van Loo<sup>4,5</sup>, Joon Jeong<sup>3</sup>, Seong-Jin Kim<sup>2,6</sup> and Seok Hee Park<sup>1,8</sup>

**Although the ubiquitin-editing enzyme A20 is a key player in inflammation and autoimmunity, its role in cancer metastasis remains unknown. Here we show that A20 monoubiquitylates Snail1 at three lysine residues and thereby promotes metastasis of aggressive basal-like breast cancers. A20 is significantly upregulated in human basal-like breast cancers and its expression level is inversely correlated with metastasis-free patient survival. A20 facilitates TGF- $\beta$ 1-induced epithelial–mesenchymal transition (EMT) of breast cancer cells through multi-monoubiquitylation of Snail1. Monoubiquitylated Snail1 has reduced affinity for glycogen synthase kinase 3 $\beta$  (GSK3 $\beta$ ), and is thus stabilized in the nucleus through decreased phosphorylation. Knockdown of A20 or overexpression of Snail1 with mutation of the monoubiquitylated lysine residues into arginine abolishes lung metastasis in mouse xenograft and orthotopic breast cancer models, indicating that A20 and monoubiquitylated Snail1 are required for metastasis. Our findings uncover an essential role of the A20–Snail1 axis in TGF- $\beta$ 1-induced EMT and metastasis of basal-like breast cancers.**

Among the six major subsets of breast carcinomas, basal-like breast cancers express basal/myoepithelial markers and are frequently triple negative for ER, PR and HER2 (ref. 1). Basal-like breast cancers are highly aggressive and have poorer prognoses than luminal subtypes<sup>2</sup>. These aggressive types frequently relapse, are more prone to metastasize to other organs, and lead to worse outcomes in breast cancer patients<sup>3,4</sup>.

A20, also called tumour necrosis factor  $\alpha$ -induced protein 3 (*TNFAIP3*), acts as a key regulator of inflammation and immunity<sup>5–9</sup>, due to its role as a nuclear factor (NF)- $\kappa$ B inhibitory and anti-apoptotic signalling protein<sup>5,10–13</sup>. Recent *in vivo* gene targeting studies indicate that A20 has cell- or disease-context-dependent functions<sup>14–21</sup>. These diverse functions may be ascribed to the ubiquitin-editing activities of A20: deubiquitylase (DUB)<sup>22–25</sup>, and E3 ubiquitin ligase activities<sup>25</sup>. A20 also acts as a ubiquitin-binding protein<sup>26,27</sup>.

Despite knowledge of the roles of A20 in inflammation and immune responses, its functions in cancer are not yet clearly understood. Several reports suggest an oncogenic role of A20 in diverse solid

tumour cell lines<sup>28–32</sup>, whereas a tumour suppressor function has been suggested for A20 in B-cell lymphoma<sup>14,33,34</sup>. Thus, A20 may play different roles in tumorigenesis through collaboration with specific oncoproteins or tumour suppressors in a context-dependent manner.

Epithelial–mesenchymal transition (EMT) is highly associated with cancer progression such as invasion and metastasis in pathological contexts<sup>35,36</sup>. Transcription factors including the Snail family (Snail1, Snail2 and Snail3), the ZEB family (ZEB1 and ZEB2) and the basic helix–loop–helix family (Twist1 and Twist2) are known as regulators driving the EMT process<sup>36,37</sup>. Among them, Snail1 is the most studied, as its expression is regulated by dual mechanisms. Snail1 is transcriptionally induced by transforming growth factor (TGF)- $\beta$  (ref. 38), hypoxia<sup>39</sup> and reactive oxygen species<sup>40</sup>. Snail1 expression is further regulated by proteasomal rapid degradation in normal cells<sup>41</sup>. Snail1 degradation is promoted by the SCF (Skp1–Cullin1–F-box)- $\beta$ -TrCP ( $\beta$ -transducin-repeat-containing protein) complex, a multi-subunit RING type E3 ubiquitin ligase, and requires phosphorylation of Snail1 by GSK3 $\beta$  as well as Lys48-linked

<sup>1</sup>Department of Biological Sciences, Sungkyunkwan University, Suwon 16419, Korea. <sup>2</sup>Precision Medicine Research Center, Advanced Institutes of Convergence Technology, Seoul National University, Suwon 16229, Korea. <sup>3</sup>Department of Surgery, Gangnam Severance Hospital, Yonsei University College of Medicine, Seoul 06273, Korea. <sup>4</sup>Inflammation Research Center, Unit of Cellular and Molecular (Patho)physiology, VIB, B-9052 Ghent, Belgium. <sup>5</sup>Department of Biomedical Molecular Biology, Ghent University, B-9052 Ghent, Belgium. <sup>6</sup>Department of Transdisciplinary Studies, Graduate School of Convergence Science and Technology, Seoul National University, Suwon 16229, Korea. <sup>7</sup>These authors contributed equally to this work.

<sup>8</sup>Correspondence should be addressed to S.H.P. (e-mail: parks@skku.edu)

polyubiquitylation<sup>41</sup>. Although A20 and Snail1 functions are well studied in inflammation and EMT, respectively, it remains unknown how A20 contributes to tumorigenesis, invasion and metastasis in conjunction with Snail1.

Here we uncover a mechanism where upregulated A20 is involved in TGF- $\beta$ -induced EMT through stabilizing Snail1 in the nucleus by multiple monoubiquitylation, thereby promoting the metastasis of aggressive basal-like breast cancers.

## RESULTS

### A20 is overexpressed in aggressive basal-like breast cancers

To identify E3 ubiquitin ligases or deubiquitylases engaged in human breast cancer metastasis, we initially performed RNA sequencing in several subtypes of human breast cancer cell lines. We found that A20 is significantly overexpressed in basal-like breast cancer cells (Fig. 1a), further supported by immunoblot analysis (Fig. 1b). The MCF10A series of cell lines, mimicking the stages of breast cancer progression from normal breast epithelial cells (M1) to highly metastatic cells (M4), showed a positive correlation between A20 expression and metastatic potential (Fig. 1c). Analysis of public microarray data sets (GSE41313) in 52 breast cancer cell lines<sup>42</sup> revealed higher expression of A20 in basal-like types, compared with luminal ones (Fig. 1d).

Analysis of The Cancer Genome Atlas (TCGA) databases and other public microarray data (GSE2034)<sup>43</sup> indicated that A20 is significantly upregulated in tumour samples of basal-like subtypes including triple-negative breast cancers (TNBCs) (Fig. 1e–g). Computational analysis of breast cancer tissue microarrays (TMAs) from Gangnam Severance Hospital in South Korea demonstrated an association of high A20 expression with distant metastasis-free, overall, and breast cancer-specific survival (Fig. 1h–j). Immunohistochemistry of the breast cancer TMAs corroborated our finding that A20 expression is higher in TNBC relative to other subtypes (Fig. 1k).

### A20 is required for TGF- $\beta$ -induced EMT

We hypothesized that A20 may be involved in TGF- $\beta$ -induced EMT, because A20 expression was increased in aggressive basal-like breast cancers. Thus, we observed morphological changes and protein levels in A20-knockdown NMuMG mouse mammary epithelial cells and MCF10A human breast epithelial cells following TGF- $\beta$ 1 treatment (Fig. 2a–e). Although TGF- $\beta$ 1 treatment induced EMT-like morphological changes in green fluorescent protein (GFP)-specific short hairpin RNA (shGFP)- or control short interfering RNA (siCON)-expressing cells, no morphological changes were observed in A20-depleted NMuMG and MCF10A cells (Fig. 2a,b). Unlike control cells, no reduction in E-cadherin expression nor increase in expression of mesenchymal markers, including N-cadherin, vimentin, fibronectin and  $\alpha$ -smooth muscle actin (SMA), was seen in A20-depleted NMuMG and MCF10A cells following TGF- $\beta$ 1 treatment (Fig. 2c–e). Such observations were further confirmed by quantitative PCR with reverse transcription (qRT-PCR) analysis of *CDH1*, *CDH2* and *VIM* messenger RNAs, which encode E-cadherin, N-cadherin and vimentin, respectively (Fig. 2f–h), and by *CDH1*-specific reporter gene analysis (Fig. 2i).

These observations prompted investigation of Snail transcription factors. Interestingly, Snail1 expression was decreased in

A20-knockdown NMuMG and MCF10A cells, while Snail2 and Twist expression was unaffected (Fig. 2d,e). A20 knockdown also reduced expression of ZEB1, possibly due to A20-mediated decrease of Snail1, which acts upstream of ZEB1 (ref. 44; Fig. 2d,e). Notably, A20 was significantly induced by TGF- $\beta$ 1 treatment in both NMuMG and MCF10A cells, with different kinetics (Fig. 2d,e). Also, immunoblot of breast cancer cell lines and surgically dissected cancer samples indicated that both A20 and Snail1 are increased in aggressive basal-like breast cancer subtypes (Fig. 2j,k). These results suggest that A20 is involved in TGF- $\beta$ 1-mediated EMT through regulation of Snail1.

### A20 stabilizes the Snail1 protein

Because Snail1 transcription is induced by the TGF- $\beta$ /Smad signalling pathway<sup>45</sup>, we examined whether A20 upregulates Snail1 through canonical TGF- $\beta$ /Smad signalling. Although Snail1 expression was reduced in A20-knockdown NMuMG or MCF10A cells, TGF- $\beta$ 1-mediated phosphorylation of Smad2/3 and expression of plasminogen activator inhibitor (*PAI*)-1, a target of TGF- $\beta$ /Smad signalling, were not affected by A20 knockdown (Fig. 3a,b). In addition, canonical TGF- $\beta$ /Smad signalling was normal in A20-knockdown NMuMG cells following TGF- $\beta$ 1 treatment as measured by the *CAGA*-luciferase reporter and *SMAD7* and *PAI1* mRNAs (Supplementary Fig. 1a–d), confirming that A20 does not regulate canonical TGF- $\beta$ /Smad signalling.

To understand how A20 regulates Snail1, we first examined *SNAIL1* mRNA in A20-knockdown NMuMG cells. Using qRT-PCR, similar *SNAIL1* expression was demonstrated following TGF- $\beta$ 1 treatment in both control and shRNA- or siRNA-induced A20-depleted NMuMG cells (Fig. 3c and Supplementary Fig. 1e). We next examined Snail1 expression in A20-knockout (*A20*<sup>-/-</sup>) mouse embryonic fibroblasts (MEFs). Compared with wild-type *A20*<sup>+/+</sup> MEFs, the Snail1 level was reduced in *A20*<sup>-/-</sup> MEF cells (Fig. 3d), whereas *SNAIL1* mRNA expression and Smad2 phosphorylation following TGF- $\beta$ 1 treatment were unaffected (Fig. 3d,e). Notably, A20 expression gradually increased in *A20*<sup>+/+</sup> MEFs during TGF- $\beta$ 1 treatment (Fig. 3d). Ectopic expression of A20 in *A20*<sup>-/-</sup> MEFs restored both A20 and Snail1 expression to levels similar to that in *A20*<sup>+/+</sup> MEFs (Fig. 3f). Cycloheximide treatment of *A20*<sup>-/-</sup> MEFs and A20-knockdown NMuMG cells further supported our results (Fig. 3g and Supplementary Fig. 1f). This decreased Snail1 stability under A20 depletion was restored by treatment with the proteasome inhibitor MG132 (Fig. 3h and Supplementary Fig. 1g). Moreover, A20 expression in HEK293 cells augmented Snail1 expression (Supplementary Fig. 1h). The regulation of Snail1 stability by A20 was also confirmed in TGF- $\beta$ 1-induced EMT of pancreatic cancers. A20-knockdown Panc-1 cells showed reduction of Snail1 and a decreased EMT phenotype in the presence of TGF- $\beta$ 1 (Supplementary Fig. 1i). Furthermore, ectopic expression of wild-type Snail1 in A20-knockdown NMuMG cells rescued EMT phenotypes including fibroblast-like morphology, decreased E-cadherin expression, and increased vimentin expression (Fig. 3i and Supplementary Fig. 1j lanes 6 and 8).

### A20 facilitates lung metastasis of aggressive breast cancer cells

Our findings led us to verify the *in vivo* functions of A20 in the pathological progression of breast cancer cells. We initially examined whether A20 affects tumour growth in cell lines and xenograft

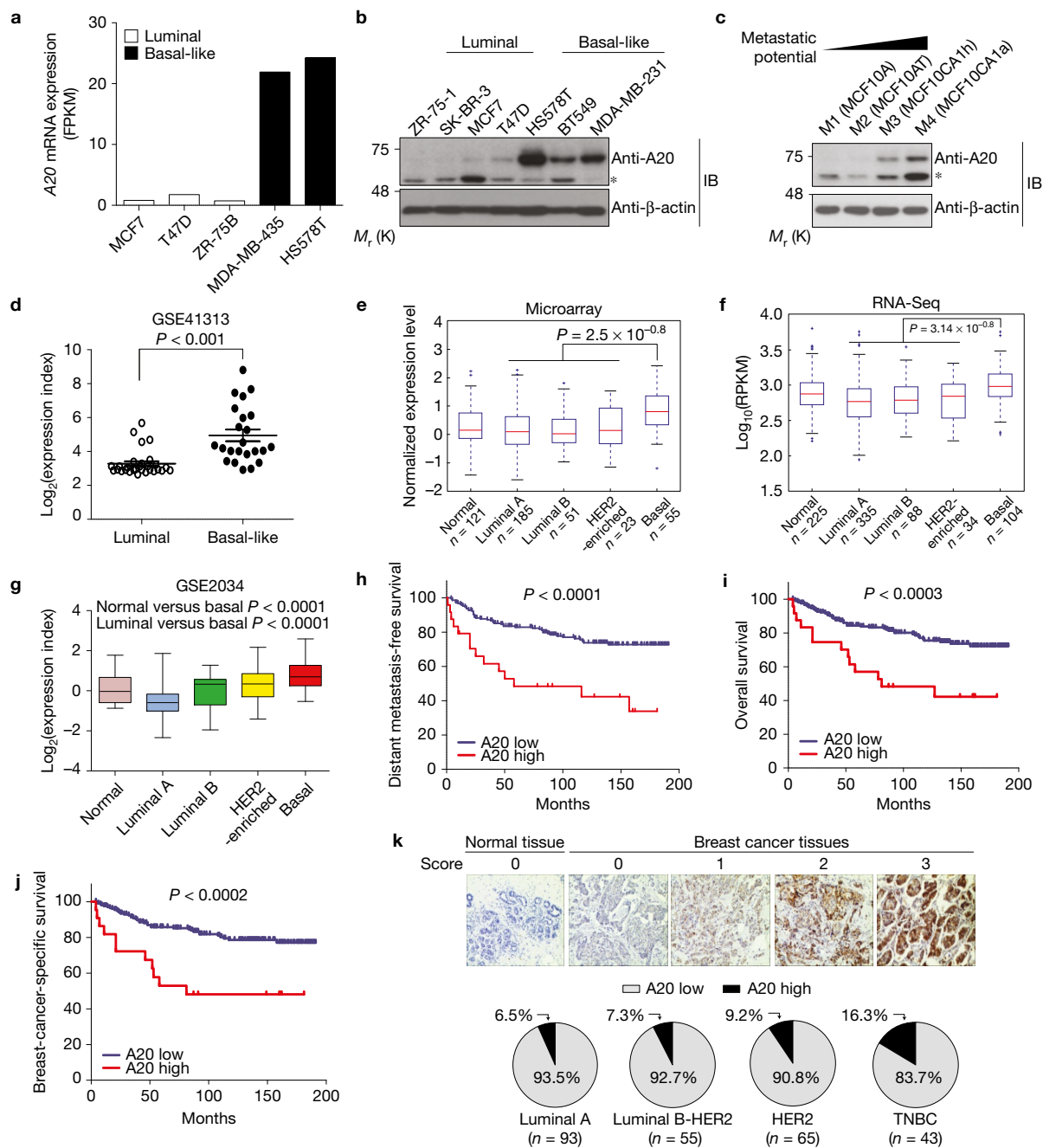


**Figure 1** Overexpression of the *A20* gene in human malignant breast cancers. (a,b) Comparison of *A20* expression levels between luminal and basal subtypes of breast cancer cells using an RNA-sequencing data set (GSE100878, a) and immunoblot analysis (b). The data in a are presented as the mean of  $n=2$  independent samples per cell line analysed. (c) Immunoblots of *A20* protein using lysates of MCF10A-derived cells with different metastatic potential. Asterisks in b,c indicate non-specific bands. The data in b,c are representative of three independent experiments and  $\beta$ -actin was used as a loading control. (d) Scatter dot plots show *A20* expression levels in 52 breast cancer cells from GEO data sets (GSE41313).  $P$  values were calculated by unpaired, two-tailed Student's  $t$ -tests. (e–g) Box plots show *A20* expression levels in breast cancer tissues of different breast cancer subtypes with those in normal tissues. Analysis of *A20* expression by microarray (normal  $n=121$ , luminal A  $n=185$ , luminal B  $n=51$ , HER2-enriched  $n=23$  and basal  $n=55$  patients) (e), and RNA sequencing (normal  $n=225$ , luminal A  $n=335$ , luminal B  $n=88$ , HER2-enriched  $n=34$  and basal  $n=104$  patients) (f) from public TCGA data sets. Analysis of *A20*

expression by microarray data from GEO data sets (GSE2034, normal  $n=53$ , luminal A  $n=95$ , luminal B  $n=25$ , HER2-enriched  $n=34$  and basal  $n=55$  patients) (g). The boxes represent the interquartile range, centre is the median, and the minimum and maximum values are represented by the whiskers.  $P$  values were calculated using unpaired, two-tailed Student's  $t$ -tests. (h–j) Correlation between *A20* expression and clinical outcomes through analysis of TMAs of breast cancer patients. A Kaplan–Meier plot analysis showed distant metastasis-free survival ( $n=236$  patients) (h), overall survival ( $n=236$  patients) (i), and breast cancer-specific survival ( $n=226$  patients) (j) depending on the expression level of *A20*.  $P$  values were calculated using a log-rank test. (k) Immunohistochemical (IHC) staining against the *A20* protein in TMAs of breast cancer patients. After scoring *A20* expression in each tissue, expression level was analysed according to breast cancer subtypes (luminal A  $n=93$ , luminal B-HER2  $n=55$ , HER2  $n=65$  and TNBC  $n=43$  patients) defined by three IHC markers (oestrogen receptor, progesterone receptor and HER2). Unprocessed original scans of blots in b,c are shown in Supplementary Fig. 9.

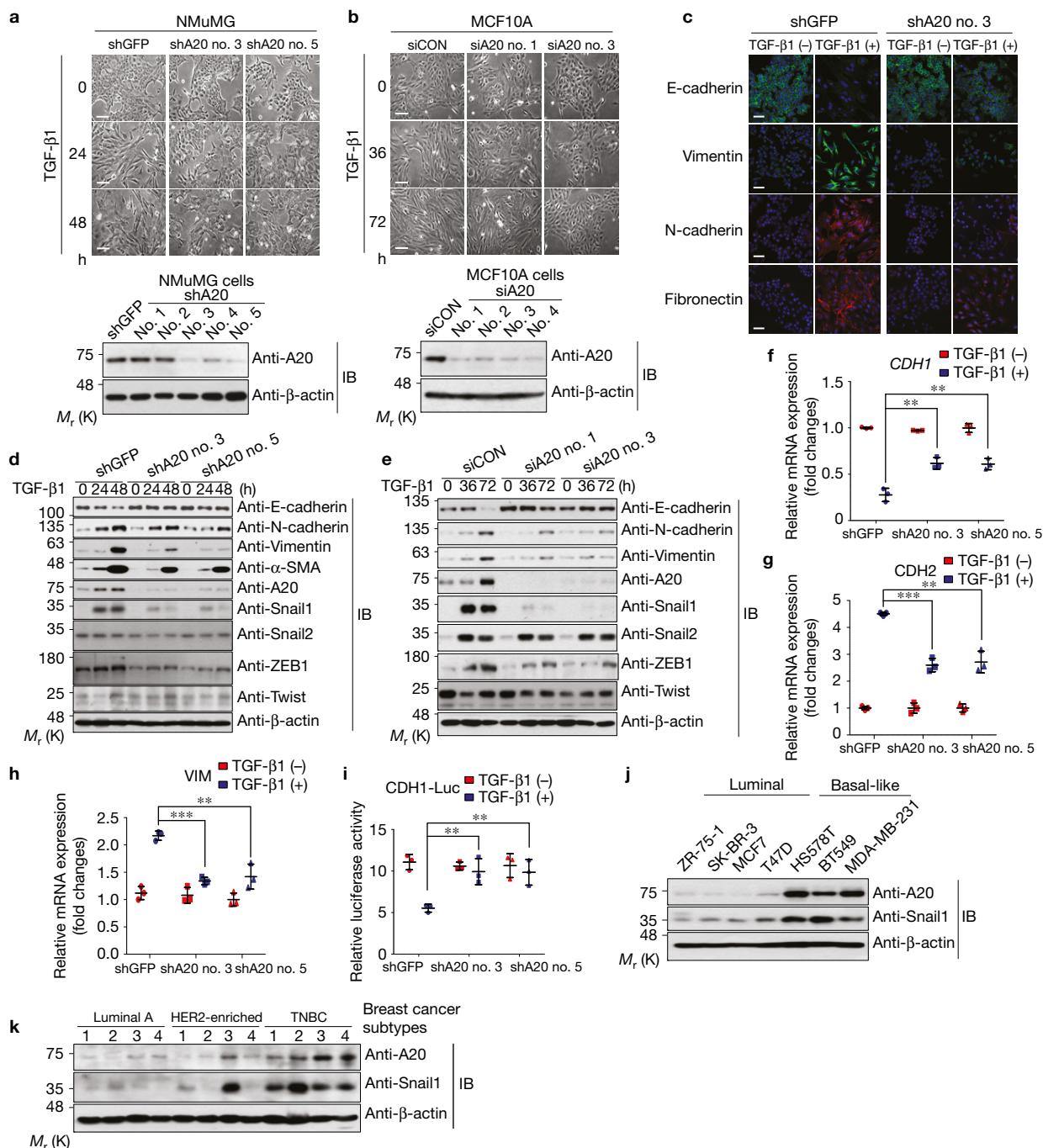


**Figure 2** A20 is involved in TGF- $\beta$ 1-induced EMT. (**a,b**) NMuMG cells (**a**), depleted by infections of lentiviruses expressing two independent shRNAs targeting *A20* mRNA (shA20 no. 3 and shA20 no. 5), and MCF10A cells (**b**), depleted by two independent *A20* siRNAs (siA20 no. 1 and siA20 no. 3), were treated with TGF- $\beta$ 1 (5 ng ml<sup>-1</sup>) for the indicated times to induce EMT. GFP-specific shRNA (shGFP) or control siRNA (siCON) was used as a negative control. Phase-contrast images of NMuMG (**a**) and MCF10A (**b**) cells were acquired at the indicated times. Scale bars, 50  $\mu$ m. Knockdown efficiency was confirmed by immunoblot analysis with anti-A20 antibody. (**c**) *A20*-knockdown NMuMG cells were treated with TGF- $\beta$ 1 for 48 h. Cells were immunostained with the indicated antibodies against EMT marker proteins. Scale bars, 50  $\mu$ m. (**d,e**) *A20*-knockdown NMuMG (**d**) or MCF10A (**e**) cells were treated with TGF- $\beta$ 1 for the indicated times. Immunoblots were performed on cell lysates with the indicated antibodies. (**f-h**) Real-time qRT-PCR was performed to analyse mRNA expression

of *CDH1* (**f**), *CDH2* (**g**) and *VIM* (**h**) in *A20*-knockdown NMuMG cells treated with TGF- $\beta$ 1 for 48 h. As a control, shGFP-expressing NMuMG cells were used. (**i**) *A20*-knockdown NMuMG cells were transfected with a *CDH1-Luc* reporter plasmid. After 24 h, cells were treated with TGF- $\beta$ 1 for 48 h and luciferase activity was measured and normalized. The data in **f-i** were statistically analysed by a *t*-test and show the mean  $\pm$  s.d. of  $n=3$  independent experiments. \*\* $P < 0.01$ , \*\*\* $P < 0.001$  compared with the shGFP control treated with TGF- $\beta$ 1. (**j,k**) Expression levels of A20 and Snail1 in breast cancer cell lines (**j**) and surgically dissected cancer samples of breast cancer patients (**k**) were observed by immunoblotting with the indicated antibodies. In all immunoblot analysis, expression of  $\beta$ -actin was used as a loading control. The data in **a-e,j-k** are representative of three independent experiments. Source data for **f-i** are available in Supplementary Table 3. Unprocessed original scans of blots in **a,b,d,e,j,k** are shown in Supplementary Fig. 9.

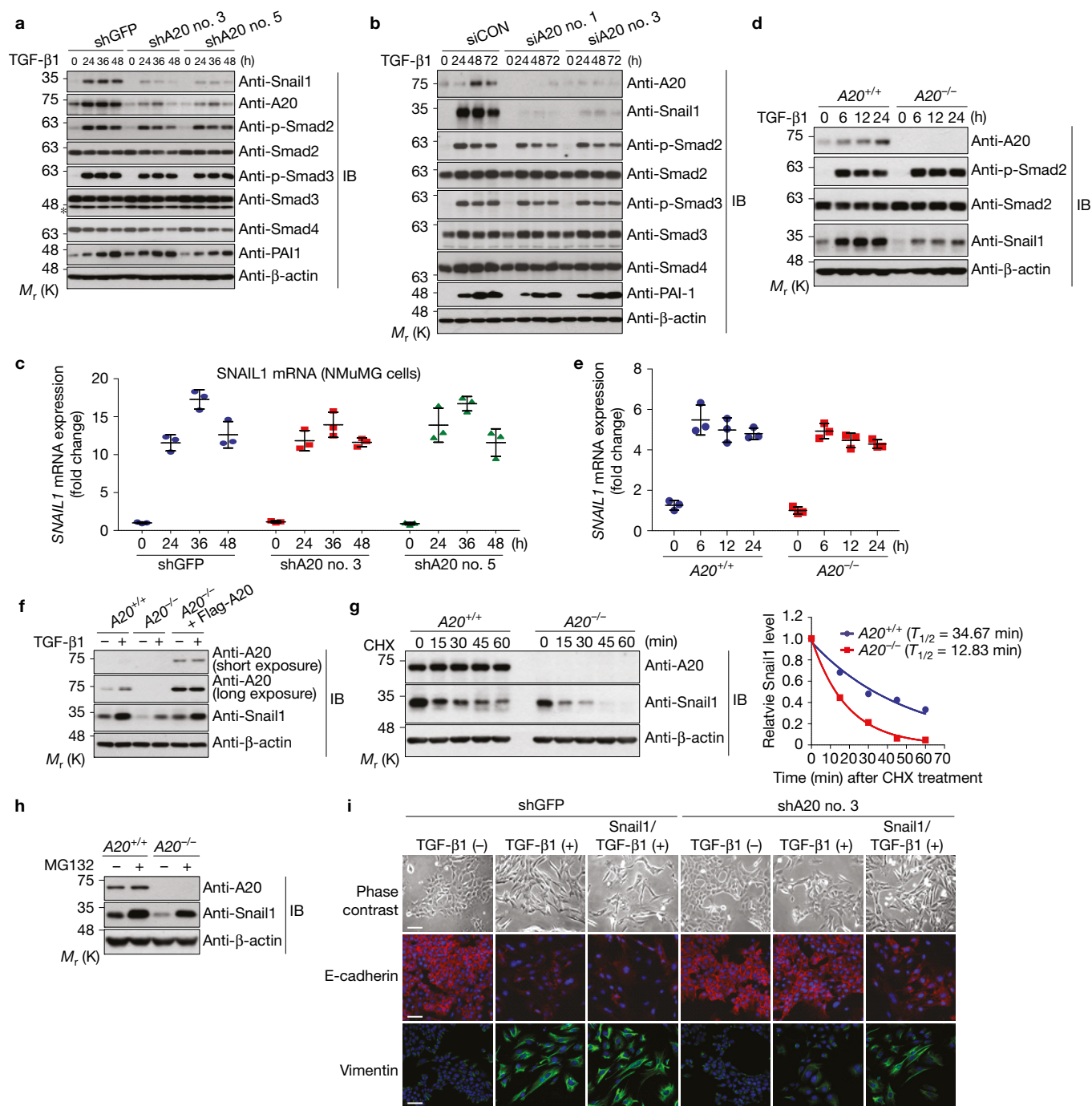


**Figure 3** Stabilization of the Snail1 protein by A20. **(a,b)** Immunoblot analysis in  $A20$ -knockdown NMuMG **(a)** or MCF10A **(b)** cells treated with TGF- $\beta$ 1 (5 ng ml $^{-1}$ ) for the indicated times. The asterisk indicates non-specific bands. **(c)** Real-time qRT-PCR to analyse expression of *SNAIL1* mRNA in  $A20$ -knockdown and control NMuMG cells treated with TGF- $\beta$ 1 for the indicated times. **(d)** Immunoblot analysis in  $A20$  wild-type ( $A20^{+/+}$ ) and  $A20$ -knockout ( $A20^{-/-}$ ) MEFs treated with TGF- $\beta$ 1 (5 ng ml $^{-1}$ ) for the indicated times. **(e)** Real-time qRT-PCR to analyse expression of *SNAIL1* mRNA in  $A20^{+/+}$  and  $A20^{-/-}$  MEFs treated with TGF- $\beta$ 1 for the indicated times. **(f)**  $A20^{-/-}$  MEFs were infected with retroviruses expressing Flag-A20 to ectopically express the A20 protein and subsequently treated with TGF- $\beta$ 1 for 24 h. Cell lysates were immunoblotted with the indicated antibodies. **(g)** The stability of the Snail1 protein was measured by immunoblots in  $A20^{+/+}$  and  $A20^{-/-}$  MEFs in the presence of cycloheximide (CHX, 50  $\mu$ g ml $^{-1}$ ) for the indicated times.

The data were quantified using ImageJ software<sup>60</sup> (right). For normalization,  $\beta$ -actin expression was used as a control. **(h)**  $A20^{+/+}$  and  $A20^{-/-}$  MEFs were treated with the proteasome inhibitor MG132 (10  $\mu$ M) for 6 h. Cell lysates were immunoblotted with the indicated antibodies. **(i)**  $A20$ -knockdown and control NMuMG cells, transfected with a plasmid encoding Flag-Snail1, were treated with TGF- $\beta$ 1 for 24 h to induce EMT. Phase-contrast images of cells were acquired and cells were immunostained with the indicated antibodies. Scale bars, 50  $\mu$ m. The data in **c** and **e** were statistically analysed by a *t*-test and show the mean  $\pm$  s.d. of  $n=3$  independent experiments. In all immunoblot analysis, expression of  $\beta$ -actin was used as a loading control. The data in **a,b,d,f-h** are representative of three independent experiments with similar results. Source data for **c,e** are available in Supplementary Table 3. Unprocessed original scans of blots in **a,b,d,f-h** are shown in Supplementary Fig. 9.

models. A20 depletion in aggressive human MCF10CA1a (M4) cells and murine mammary carcinoma 4T1-Luc cells did not significantly change cell numbers and tumour sizes (Supplementary Fig. 2). We next investigated whether A20 influences the invasion of M4 and 4T1-Luc cells with Matrigel invasion and Transwell migration assays. A20 depletion decreases the invasiveness of M4 and 4T1-Luc cells (Fig. 4a–c). Since A20 depletion in M4 and 4T1-Luc cells also increased expression of E-cadherin and reduced vimentin (Supplementary Fig. 2a,e), we examined the role of A20 in the malignant progression of aggressive breast cancer cells. A20 depletion significantly reduced lung metastasis of M4 cells that had been injected into the tail vein of SCID mice (Fig. 4d,e). A pro-metastatic effect of A20 was also confirmed by *in vivo* imaging of dramatically decreased lung metastases (Fig. 4f) and a reduced number of metastatic pulmonary nodules of A20-depleted 4T1-Luc cells at 35 day post-injection (Fig. 4g,h).

### A20 monoubiquitylates multiple sites of Snail1

To examine how A20 molecularly promotes metastasis of aggressive breast cancers, we checked the interaction between A20 and Snail1. Immunoprecipitation assay against endogenous proteins as well as co-immunoprecipitation indicated that A20 specifically binds to Snail1 (Fig. 5a,b). The endogenous interaction between these two proteins was notably increased following TGF- $\beta$ 1 treatment (Fig. 5b).

Considering the ubiquitin-editing activities of A20, we examined the ubiquitylation pattern of Snail1. Pulldown experiments revealed that ectopically overexpressed A20 induces Snail1 bands of higher molecular weights corresponding to Snail1 with one or two ubiquitins (Fig. 5c). By contrast, polyubiquitylation patterns, induced by co-expression of HA-GSK3 $\beta$  and HA- $\beta$ TrCP1, were not detected for Snail1 in the presence of A20 (Supplementary Fig. 3a). Pulldown assays using the 7KR ubiquitin mutant (His-Ub7KR) where all seven lysines were mutated to arginines, revealed two shifted bands, indicating the conjugation of 7KR ubiquitin mutants to Snail1 (Fig. 5d). In the absence of A20 overexpression, a shifted band for Snail1 of size corresponding to monoubiquitylated Snail1 was still detected. To check whether endogenous A20 is responsible for the shifted band of Snail1, we reconstituted murine A20-depleted NMuMG cells with a plasmid encoding human A20 (HA-A20) and conducted a pulldown assay. The human A20 gene was not depleted by the shRNA targeting murine A20 mRNA in NMuMG cells. The shifted Snail1 bands disappeared following A20 depletion, and reappeared following reconstitution of A20 expression (Fig. 5e). An immunoprecipitation assay revealed a strong interaction between Snail1 and A20 at 12 h after TGF- $\beta$ 1 treatment, suggesting that Snail1 monoubiquitylation by A20 is initiated between 6 h and 12 h (Supplementary Fig. 3b). *In vitro* ubiquitylation assay also provided evidence that Snail1 monoubiquitylation is directly mediated by A20 (Fig. 5f). Snail1 has been reported to be polyubiquitylated only by SCF (Skp1–Cullin1–F-box) E3 ubiquitin ligases including SCF- $\beta$ -TrCP1, and Snail1 polyubiquitylation induces its proteasomal degradation<sup>36,41,46</sup>. Therefore, our finding firmly establishes Snail1 monoubiquitylation.

To confirm which domain of A20 is responsible for Snail1 monoubiquitylation, we generated A20 mutants where key residues in the ZnF4 and ZnF7 domains were substituted with alanines<sup>25,27</sup>. Pulldown assays using these A20 mutants indicated that Snail1 monoubiquitylation is decreased in the A20(F770A/G771A) and

A20(4A;Y614A/F615A/F770A/G771A) mutants, whereas the A20(C624A/C627A) mutant did not reduce Snail1 monoubiquitylation to the extent of the A20(F770A/G771A) mutant (Fig. 5g). Because the A20(F770A/G771A) mutant (HA-A20\_ZnF7\*) still bound to A20 protein (Supplementary Fig. 3c), the reduction of Snail1 monoubiquitylation by this mutant was not caused by the loss of binding with Snail1. These results suggest that the F770 and G771 of the ZnF7 domain are crucial for Snail1 monoubiquitylation. Consistently, the ZnF7 domain directly mediated Snail1 monoubiquitylation in an *in vitro* ubiquitylation assay. The A20(F770A/G771A) mutant (GST-A20\_ZnF7\*) did not monoubiquitylate Snail1, while wild-type A20 (GST-A20\_WT) did without promoting Snail1 polyubiquitylation (Supplementary Fig. 3d). Treatment with cycloheximide indicated that Snail1 protein stability was decreased in the presence of the A20(F770A/G771A) mutant (Fig. 5h).

Next, we investigated whether monoubiquitylation levels affect Snail1 stabilization. Treatment of a DUB inhibitor G5 indicated that Snail1 expression and monoubiquitylation levels were increased (Supplementary Fig. 3e). To check whether Snail1 stabilization might be due to the DUB activity of A20 targeting  $\beta$ -TrCP1-mediated Snail1 polyubiquitylation, pulldown assays in NMuMG cells pretreated with MG132 were performed. Snail1 polyubiquitylation by GSK3 $\beta$  and  $\beta$ -TrCP1 was not affected by ectopic A20 expression (Supplementary Fig. 3f). Expression of the HA-A20(C103A) mutant<sup>47</sup> with impaired DUB activity did not increase Snail1 polyubiquitylation. These results suggest that the DUB activity of A20 is not involved in Snail1 stabilization.

### Three monoubiquitylated Snail1 lysine residues are critical for metastasis

Snail1 contains 14 lysine residues distributed in amino (N)-terminal serine-rich and carboxy (C)-terminal zinc-finger domains (Fig. 6a). To determine which lysine residues are critical for A20-mediated Snail1 monoubiquitylation, we initially generated two Snail1 mutants, Snail1(N-6KR) and Snail1(C-8KR) (Fig. 6a). After these mutants were transiently transfected into NMuMG cells in the absence or presence of A20, pulldown assays were performed (Supplementary Fig. 4a). While wild-type Snail1 and the Snail1(N-6KR) mutant behaved similarly, the Snail1(C-8KR) mutant did not undergo monoubiquitylation or increase stability by A20 (Supplementary Fig. 4a). Therefore, monoubiquitylation sites of Snail1 by A20 are probably localized in the zinc-finger domain. The Snail1(N-6KR) mutant was not stabilized by A20 although monoubiquitylation was observed (Supplementary Fig. 4a lane 5). This could be explained by the intrinsic instability of the Snail1(N-6KR) mutant, evidenced by its extremely low expression in the absence of A20 (Supplementary Fig. 4a lane 2). We subsequently generated single lysine-to-arginine mutants of Snail1 and examined the stability of these mutants in the presence of A20 (Supplementary Fig. 4b). Snail1(K206R) and Snail1(K234,235R) mutants showed decreased expression in the presence of A20 (Supplementary Fig. 4b), suggesting that Lys206, Lys234 and Lys235 of Snail1 are potential monoubiquitylation sites by A20.

Therefore, we generated a Snail1(3KR) mutant (K206R/K234R/K235R). Pulldown assays indicated that the Snail1(3KR) mutant is not monoubiquitylated by A20 and its expression is decreased, similar to the Snail1(C-8KR) mutant (Fig. 6b). Cycloheximide treatment showed

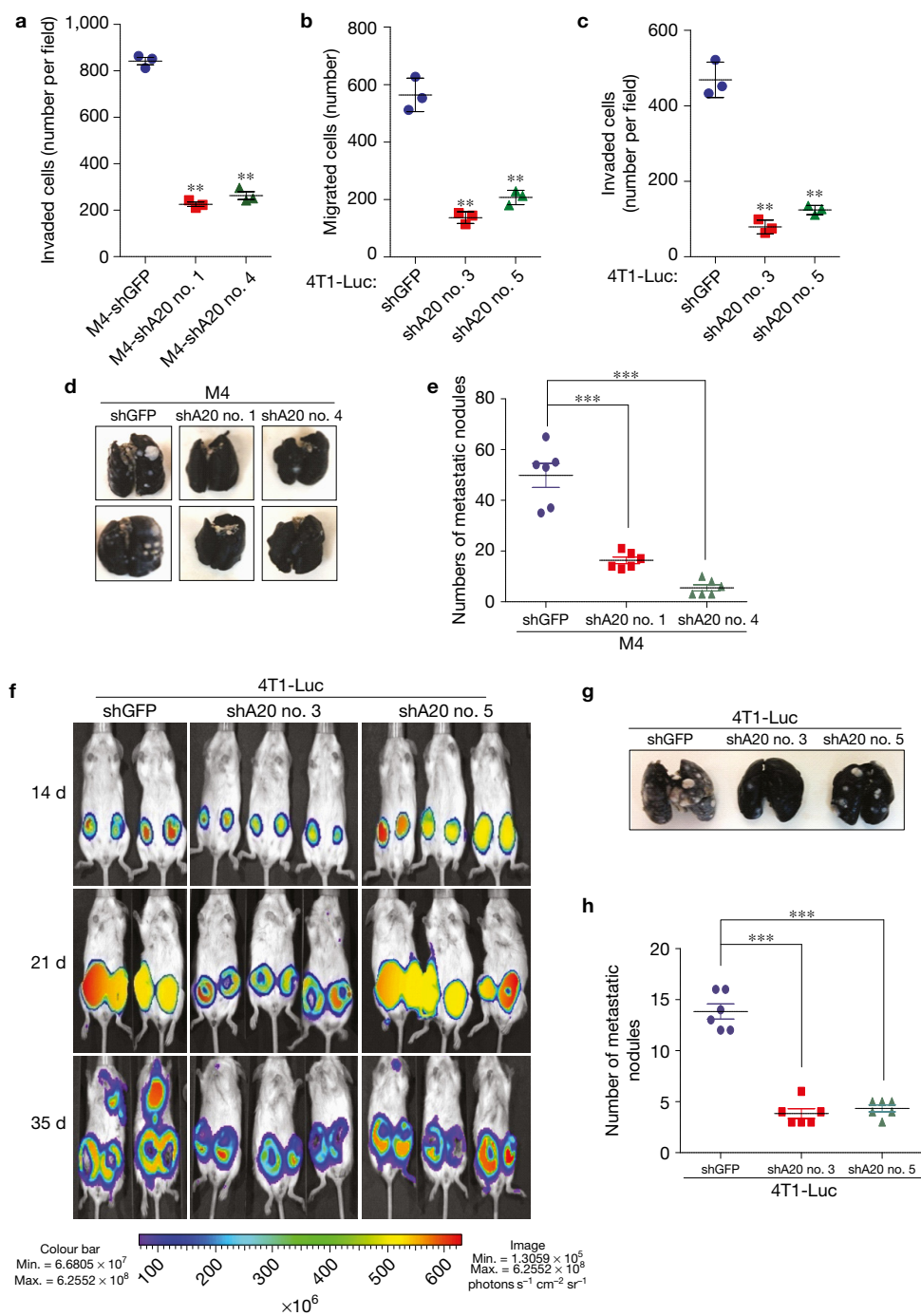


**Figure 4** A20 promotes the metastasis of aggressive breast cancer cells. **(a)** A20-knockdown MCF10CA1a (M4) cells or shGFP-expressing control cells were seeded for invasion assays. After 48 h, invading cells across the Matrigel were stained with haematoxylin and counted. **(b,c)** A20-knockdown or shGFP-expressing control 4T1-Luc cells were seeded for Transwell migration and invasion assays. After 24 h, migrating cells across the chamber **(b)** or invading cells across the Matrigel **(c)** were stained with haematoxylin and counted. The data in **a–c** were statistically analysed by a *t*-test and show the mean  $\pm$  s.d. of  $n=3$  independent experiments.  $**P < 0.01$  compared with the shGFP-expressing control M4 or 4T1-Luc cells. **(d,e)**  $5 \times 10^5$  of A20-knockdown MCF10CA1a (M4) cells were tail-vein injected into NOD/SCID mice ( $n=6$  mice per group). After the mice were euthanized 5 weeks later, lungs were removed and stained with India ink. As a control, the same amounts of shGFP-expressing M4 cells were

tail-vein injected into the mice ( $n=6$  mice). Representative images of lung metastatic nodules are shown in **d** and the numbers of metastatic nodules were measured **(e)**. **(f–h)**  $5 \times 10^4$  of A20-knockdown 4T1-Luc cells were orthotopically injected into the mammary fat pads of Balb/c mice ( $n=6$  mice per group). After injection, bioluminescence images were monitored at the indicated time points **(f)**. After the mice were euthanized 5 weeks later, lungs were removed and stained with India ink. Representative images of lung metastatic nodules are shown in **g** and the numbers of metastatic nodules were measured **(h)**. As a control, the same amounts of shGFP-expressing 4T1-Luc cells were orthotopically injected into mice ( $n=6$ ). The data in **e** and **h** were statistically analysed by a *t*-test and show the mean  $\pm$  s.d.  $n=6$  mice per group.  $***P < 0.001$  compared with the shGFP-expressing control M4 or 4T1-Luc cells. Source data for **a–c,e,h** are available in Supplementary Table 3.

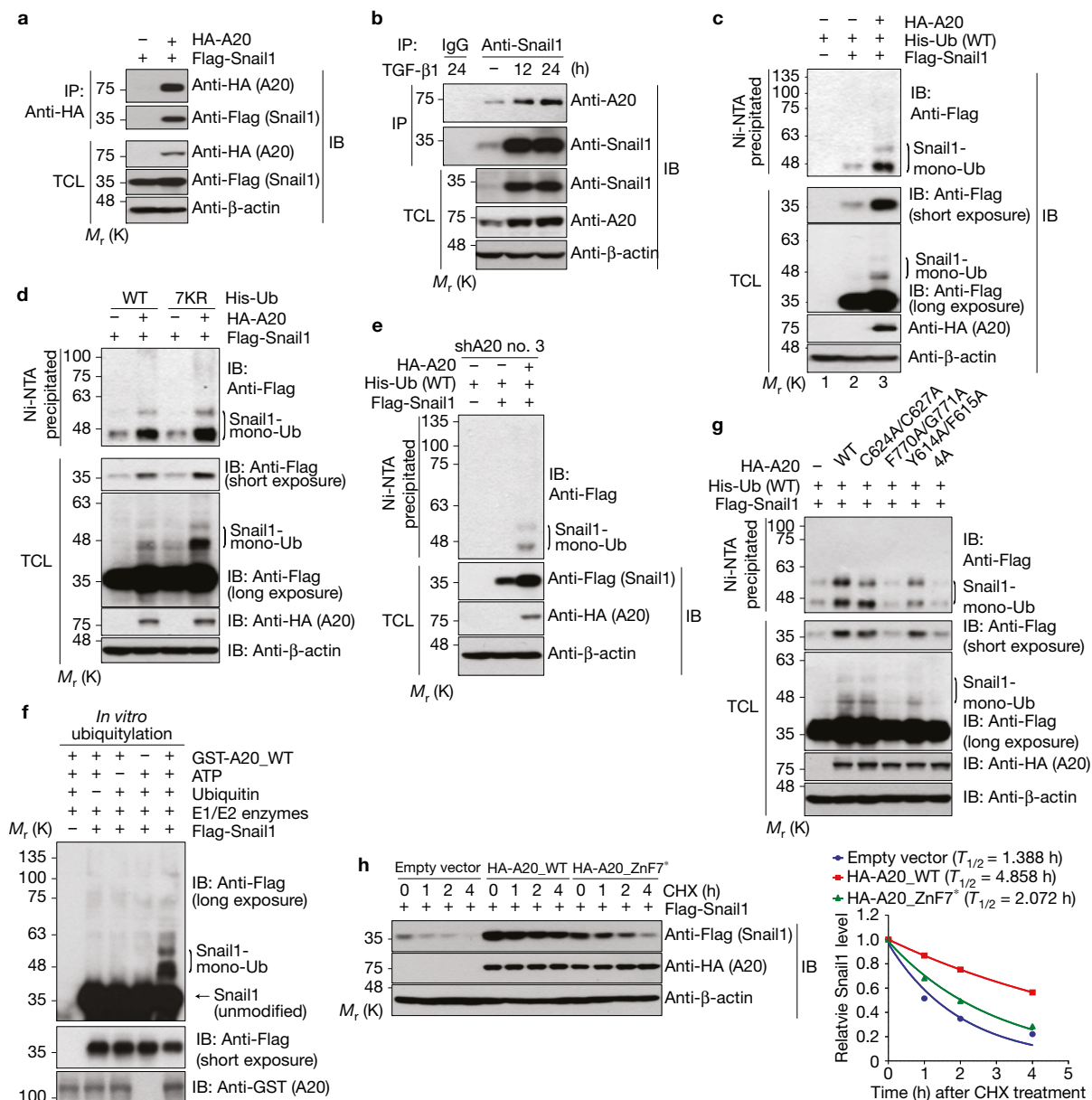


**Figure 5** The ZnF7 domain of A20 induces the monoubiquitylation of Snail1. **(a)** Co-immunoprecipitation assay in HEK293 cells co-transfected with Flag-Snail1 and HA-A20 plasmids. TCL, total cell lysates. **(b)** Immunoprecipitation assay in NMuMG cells, treated with TGF-β1 for the indicated times, with anti-Snail1 antibody. **(c,d)** After a plasmid encoding wild-type **(c)** or a lysine mutant (7KR) **(d)** of His-Ub was co-transfected with Flag-Snail1 plasmid into NMuMG cells in the absence or presence of HA-A20, Ni-NTA-mediated pulldown assays were performed. **(e)** Plasmids encoding Flag-Snail1 and wild-type His-Ub were co-transfected into A20-knockdown NMuMG cells with shRNA-resistant human HA-A20 in the indicated combinations. Ni-NTA-mediated pulldown assays were performed. **(f)** For *in vitro* ubiquitylation assays, Flag-Snail1 proteins were eluted from HEK293 cells transfected with Flag-Snail1 plasmid, and GST-A20 proteins were purified from *Escherichia coli*. The reactions were performed in the presence of the E1 and E2 enzymes as indicated and samples were

immunoblotted with the indicated antibodies. **(g)** Plasmids encoding wild-type A20 or A20 mutants (C624A/C627A, F770A/G771A, Y614A/F615A, 4A: Y614A/F615A/F770A/G771A) were co-transfected with Flag-Snail1 and wild-type His-Ub plasmids into NMuMG cells in the indicated combinations. Ni-NTA-mediated pulldown assays were performed. Ubiquitylated Snail1 in the data **(c–g)** was observed by immunoblotting using anti-Flag antibody. **(h)** Plasmids expressing wild-type A20 (HA-A20) or the ZnF7\* mutant (HA-A20\_ZnF7\*; F770A/G771A) were co-transfected with Flag-Snail1 plasmid into NMuMG cells in the presence of CHX (50 μg ml<sup>-1</sup>) for the indicated times. Cell lysates were immunoblotted by antibodies as indicated (left). The data were quantified using ImageJ software (right). For normalization, β-actin expression was used as a control. In all immunoblot analysis, expression of β-actin was used as a loading control except for **f**. The data are representative of three independent experiments with similar results. Unprocessed original scans of blots in Fig. 5 are shown in Supplementary Fig. 9.

that the stability of the Snail1(3KR) mutant was decreased even in the presence of A20 (Fig. 6c). Lys206, Lys234 and Lys235 of Snail1 are evolutionarily conserved in other species (Fig. 6d).

We next examined whether A20-mediated monoubiquitylation of Snail1 is linked to other mechanisms stabilizing Snail1, since Snail1 is reportedly stabilized through phosphorylation at Ser82

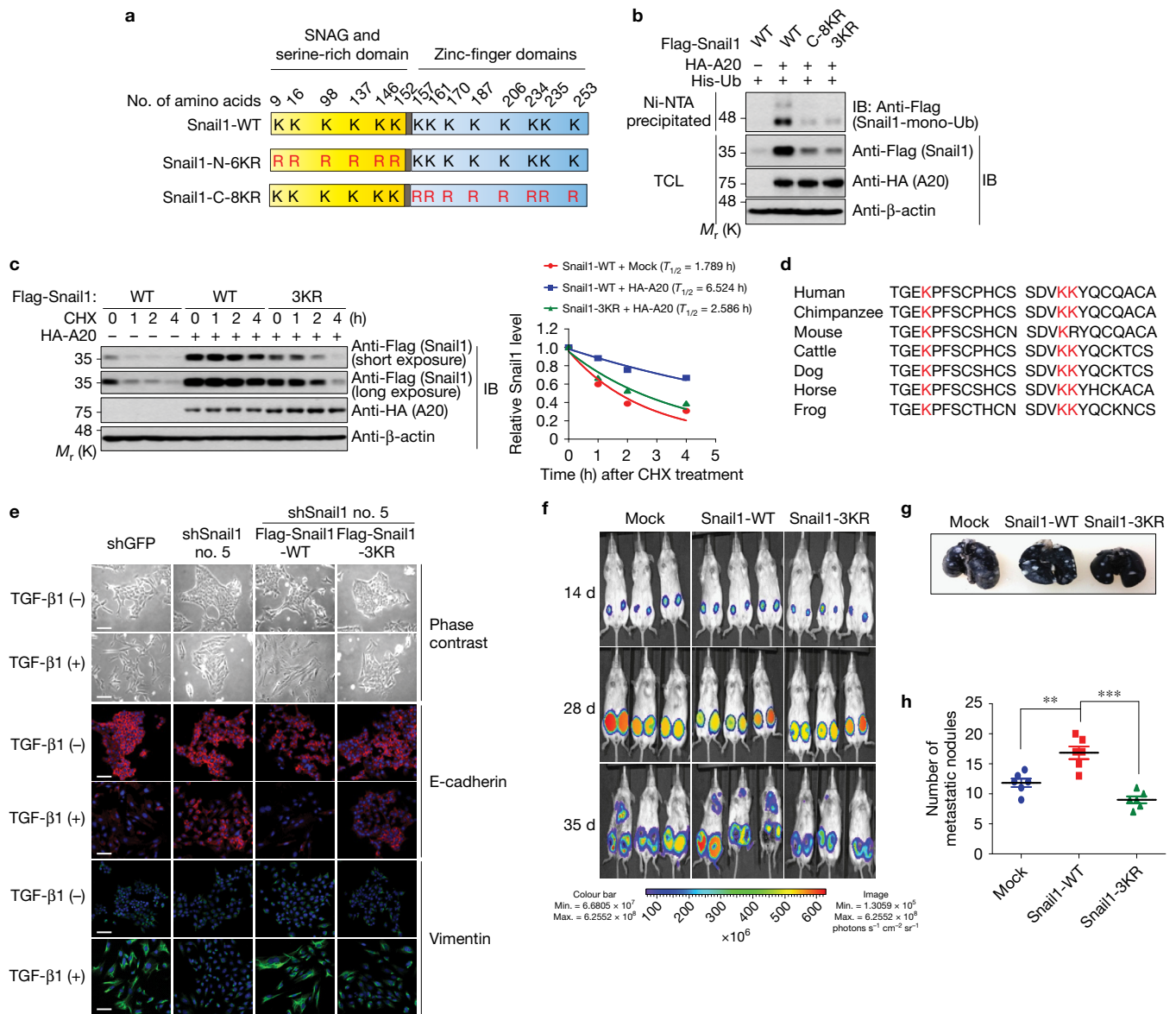


**Figure 6** Three lysine residues of Snail1 monoubiquitylated by A20 are critical for metastasis. **(a)** Schematic diagram of Snail1 mutants. **(b)** Ni-NTA pulldown assays in NMuMG cells transfected with a plasmid expressing wild-type Snail1 or Snail1 mutants (C-8KR and 3KR) together with His-Ub and HA-A20. Ubiquitylated Snail1 was observed by immunoblotting using an anti-Flag antibody. β-actin expression was used as a loading control. **(c)** A plasmid encoding Flag-Snail1 or Flag-Snail1-3KR was co-transfected into NMuMG cells with or without HA-A20. Cells were treated with cycloheximide (CHX, 50 μg ml<sup>-1</sup>) for the indicated times. Cell lysates were immunoblotted with the indicated antibodies (left). The data were quantified using ImageJ software (right). For normalization, β-actin expression was used as a control. **(d)** Conservation of Snail1 lysine residues at amino acids 206, 234 and 235 in diverse species. **(e)** NMuMG cells, depleted by shRNAs (shSnail1 no. 5) specific to mouse *SNAIL1* mRNA, were reconstituted by infection with retroviruses expressing wild-type or the 3KR mutant of human Snail1. shGFP-expressing NMuMG cells were used as a

control. Cells were treated with TGF-β1 for 48 h. Phase-contrast images of NMuMG cells were acquired and cells were immunostained with the indicated antibodies. Scale bars, 50 μm. **(f–h)** 5 × 10<sup>4</sup> 4T1-Luc cells, infected with retroviruses expressing wild-type Snail1 or Snail1-3KR mutant, were injected into Balb/c mice (n = 6 mice per group). As a control, the same amounts of 4T1-Luc cells infected with retroviruses expressing empty vector (Mock) were used. Bioluminescence imaging was monitored at the indicated time points **(f)**. Lungs were removed five weeks later and stained with India ink. Representative images of lung metastatic nodules are shown in **g** and the numbers of metastatic nodules were measured **(h)**. The data in **h** were statistically analysed by a *t*-test and show the mean ± s.d. n = 6 mice per group. \*\**P* < 0.01 and \*\*\**P* < 0.001 compared with wild-type Snail1-expressing 4T1-Luc cells. Images in **b, c, e** are representative of three independent experiments. Source data for **h** are available in Supplementary Table 3. Unprocessed original scans of blots in **b, c** are shown in Supplementary Fig. 9.

and Ser104 by ERK<sup>48</sup>. A phosphorylation-incapable Snail1 mutant (Flag-Snail1(S82A/S104A)) was stabilized by A20 to levels similar to that of wild type (Supplementary Fig. 4c). Thus, A20-mediated Snail1 stabilization is not due to ERK phosphorylation.

We also investigated whether Snail1 monoubiquitylation by A20 is crucial for TGF-β-induced EMT and metastasis of aggressive breast cancers. We established *Snail1*-knockdown NMuMG cells using shRNAs (Supplementary Fig. 4d) and examined TGF-β-induced

EMT after re-expression of wild-type Snail1 or Snail1(3KR) mutant. In contrast to the wild-type Snail1, the 3KR mutant failed to restore cellular changes following TGF- $\beta$ 1 treatment despite comparable protein levels (Fig. 6e and Supplementary Fig. 4e,f). Next, we examined the metastatic potential of Snail1 monoubiquitylation in an orthotopic 4T1-Luc breast cancer model by using 4T1-Luc cells expressing Snail1(WT) or the 3KR mutant (Supplementary Fig. 5a). Wild-type Snail1-expressing 4T1-Luc cells metastasized into lungs more rapidly than the control cells, whereas metastasis of 3KR mutant-expressing cells was reduced during the same time (Fig. 6f). Consistently, a reduction in metastatic pulmonary nodules was observed in mice injected with 3KR mutant-expressing cells (Fig. 6g,h). The 3KR mutant-expressing cells did not affect tumour growth in a xenograft model (Supplementary Fig. 5b,c). *In vivo* reconstitution experiments in additional combinations in the orthotopic 4T1-Luc breast cancer model further supported the crucial role of the A20–Snail1 axis in the metastasis of aggressive breast cancers (Supplementary Fig. 5d–h).

### Snail1 monoubiquitylation by A20 inhibits GSK3 $\beta$ -mediated Snail1 phosphorylation

To understand the importance of A20-mediated Snail1 monoubiquitylation in the regulation of EMT and metastasis, we turned to GSK3 $\beta$ , which induces Snail1 phosphorylation and nuclear export, ultimately resulting in the degradation of Snail1 through the ubiquitin ligase SCF- $\beta$ -TrCP1 (refs 36,41). A20 did not bind to GSK3 $\beta$  (Supplementary Fig. 6a), contrary to the A20 binding to Snail1 (Fig. 5a,b). However, ectopic expression of A20 simultaneously increased Snail1 stability and decreased the interaction between Snail1 and specifically GSK3 $\beta$  (Fig. 7a, lanes 2 and 3), but not protein kinase D1 (PKD1) (Fig. 7a lanes 5 and 6), which can induce Snail1 phosphorylation<sup>49</sup>. TGF- $\beta$ 1-induced expression of endogenous A20 reduced Snail1 interaction with GSK3 $\beta$  and A20 depletion enhanced the GSK3 $\beta$ –Snail1 interaction (Fig. 7b). The stronger binding of GSK3 $\beta$  with Snail1 following A20 depletion may accelerate Snail1 degradation through increased Snail1 phosphorylation.

Next, we examined the potential role of A20-mediated Snail1 monoubiquitylation in the interaction between Snail1 and GSK3 $\beta$ . While the binding of wild-type Snail1 protein with GSK3 $\beta$  was reduced in the presence of A20 (Fig. 7c, lanes 2 and 3), the Snail1(3KR) mutant comparatively showed stronger binding with GSK3 $\beta$  regardless of the presence of A20 (Fig. 7c, lanes 4 and 5). The reduced expression of the 3KR mutant was restored in the presence of LiCl, a GSK3 $\beta$  inhibitor (Fig. 7d, lanes 3 and 5).

Nuclear and cytoplasmic fractionation of wild-type Snail1- or Snail1(3KR) mutant-expressing NMuMG cells showed that a considerable amount of wild-type Snail1 was localized in the nucleus in the presence of A20 (Fig. 7e, lanes 2 and 8) whereas nuclear localization of the 3KR mutant was reduced in the nucleus even in the presence of A20 (Fig. 7e, lanes 8 and 11). Immunofluorescence analysis confirmed the localization of the 3KR mutant (Supplementary Fig. 6b). However, GSK3 $\beta$  inhibition restored expression of both wild-type Snail1 and the 3KR mutant (Fig. 7e), demonstrating that A20-mediated Snail1 monoubiquitylation is critical to decrease Snail1 and GSK3 $\beta$  interaction, augmenting Snail1 stability.

We further assessed the relationship between GSK3 $\beta$ -mediated phosphorylation and A20-mediated monoubiquitylation of Snail1 (Fig. 7f). A20 expression decreased the phosphorylation of wild-type Snail1 by GSK3 $\beta$ , whereas the 3KR mutant showed increased phosphorylation even in the presence of A20 (Fig. 7f, lanes 3 and 6). Increased phosphorylation of the 3KR mutant caused translocation from the nucleus into the cytoplasm for degradation by SCF- $\beta$ -TrCP1, as confirmed by treatment with leptomycin B (Fig. 7g, lanes 11 and 12), a nuclear export inhibitor, and  $\beta$ -TrCP1 depletion (Supplementary Fig. 6c,d). Immunofluorescence indeed revealed that both Snail1 and A20 translocate and co-localize in the nucleus of shGFP-expressing control NMuMG cells following TGF- $\beta$ 1 treatment (Fig. 7h). However, nuclear Snail1 was significantly decreased in A20-knockdown NMuMG cells even in the presence of TGF- $\beta$ 1 and this decreased expression was restored by MG132 treatment (Fig. 7h and Supplementary Fig. 6e). Co-immunoprecipitation and chromatin immunoprecipitation assays revealed that the Snail1(3KR) mutant shows decreased interaction with the transcriptional co-repressors HDAC1, HDAC2 and Sin3A without the loss of DNA binding activity (Supplementary Fig. 6f,g).

### A20 is required for cancer stemness and chemoresistance

Although EMT has been considered as a major mechanism for cancer metastasis, recent studies demonstrate that EMT induces cancer stemness and chemoresistance<sup>50,51</sup>. To understand the role of A20 in EMT-induced cancer stemness and chemoresistance, we generated A20-depleted M4 and MDA-MB-231 cells. Mammosphere and fluorescence-activated cell sorting (FACS) analyses revealed that the mammosphere formation and CD44<sup>+</sup>/CD24<sup>-</sup> cancer cell population are decreased in A20-depleted M4 breast cancer cells (Fig. 8a,b and Supplementary Fig. 7a), compared with control cells. In addition, A20-depleted MDA-MB-231 and M4 cells significantly reduced cell viability following treatment with anti-cancer drugs, doxorubicin and docetaxel (Fig. 8c).

### A20 is involved in TNF- $\alpha$ -mediated Snail1 stabilization

The fact that the inflammatory cytokine TNF- $\alpha$  induces A20 (refs 10,11) and stabilizes Snail1 (refs 52,53) raised the possibility that A20 may contribute to inflammation-induced EMT by TNF- $\alpha$ . To examine this possibility, stable cell lines expressing Snail1 in A20<sup>-/-</sup> MEFs as well as A20<sup>+/+</sup> MEFs were treated with TNF- $\alpha$ . Whereas Snail1 expression increased following TNF- $\alpha$  treatment in A20<sup>+/+</sup> MEFs, Snail1 expression was decreased in A20<sup>-/-</sup> MEFs (Fig. 8d) and restored by MG132 pre-treatment (Fig. 8e, lanes 2 and 4). Additionally, considerable amounts of Snail1 were translocated to the nucleus of A20<sup>+/+</sup> MEFs (Fig. 8f), similar to TGF- $\beta$ 1 treatment (Fig. 7g). A20-depleted HS578T cells, a TNBC cell line with mesenchymal features, showed decreased levels of Snail1 and N-cadherin proteins following TNF- $\alpha$  or TGF- $\beta$ 1 treatment, but no change in *SNAIL1* mRNA levels (Fig. 8g,h). However, TNF- $\alpha$ -induced Snail1 stabilization is probably distinct from the TGF- $\beta$ 1-induced one. The major difference is the kinetics of A20 induction; 24 h post-TGF- $\beta$ 1 treatment versus 6 h post-TNF- $\alpha$  treatment in MEF and HS578T cells (Figs 3d and 8d,g). Indeed, the analysis of the GEO data set GSE41970 (ref. 54) covering mRNA expression of different TNBC stage patients may support different expression kinetics of two cytokines. In this data set, TNF- $\alpha$  expression

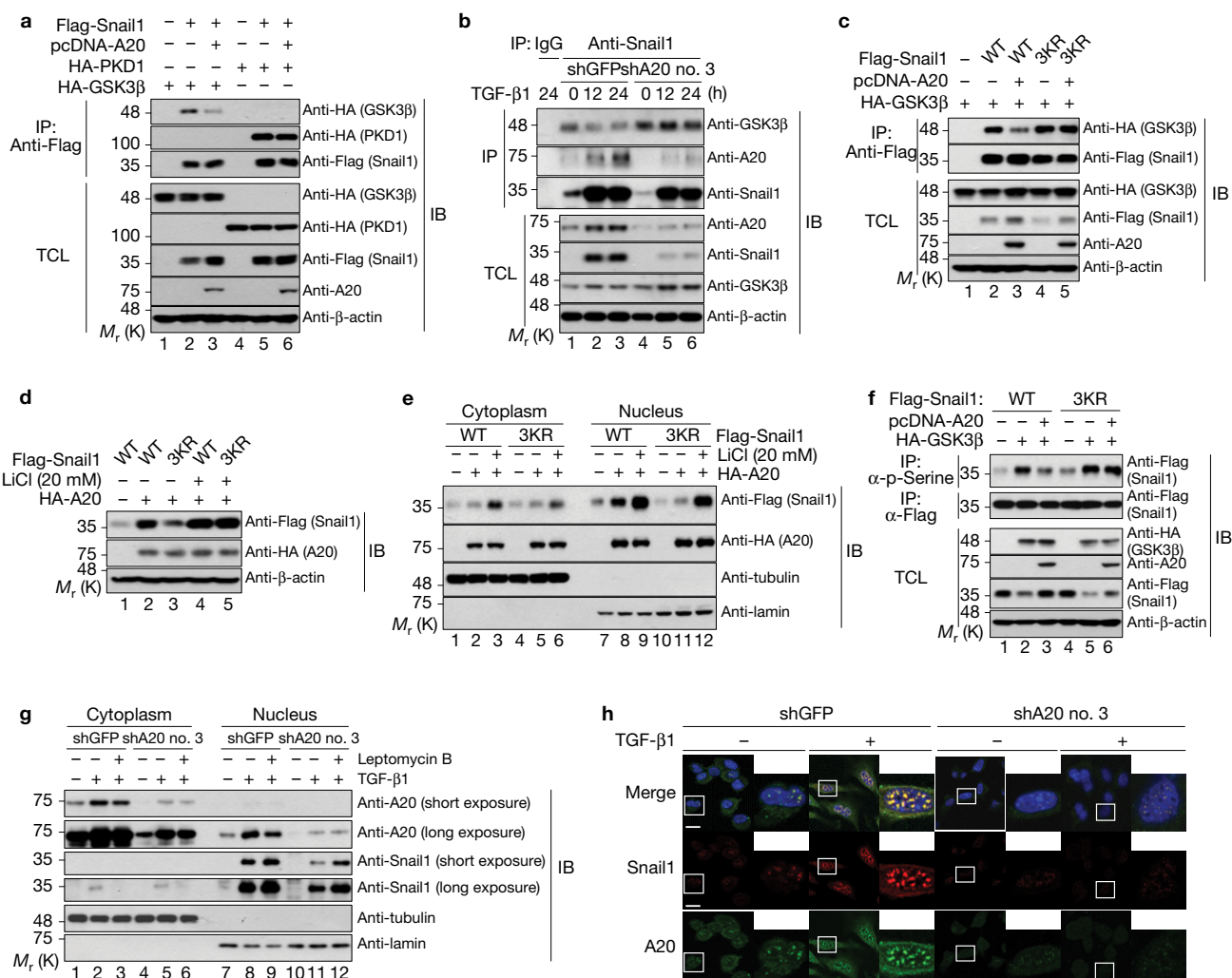


**Figure 7** A20 retains Snail1 protein in the nucleus through inhibition of GSK3 $\beta$ -mediated Snail1 phosphorylation. **(a)** Co-immunoprecipitation assay in NMuMG cells co-transfected with Flag-Snail1, HA-PKD1, HA-GSK3 $\beta$  and pcDNA-A20 plasmids in the indicated combinations. **(b)** To analyse time-dependent interactions of endogenous A20, Snail1 and GSK3 $\beta$  protein, A20-knockdown and control NMuMG cells were treated with TGF- $\beta$ 1 (5 ng ml $^{-1}$ ) for the indicated times. Cell lysates were immunoprecipitated with anti-Snail1 antibody and immunoblotted. **(c)** Plasmids encoding WT Flag-Snail1 or Flag-Snail1-3KR mutant were co-transfected with HA-GSK3 $\beta$  into NMuMG cells in the absence or presence of pcDNA-A20. Cell lysates were immunoprecipitated with anti-Flag antibody and immunoblotted. **(d,e)** Plasmids encoding wild-type Flag-Snail1 or Flag-Snail1-3KR were co-transfected with HA-A20 into NMuMG cells, which were treated with LiCl (20 mM) for 5 h. Cell lysates were immunoblotted with the indicated antibodies **(d)**. Cells were fractionated into cytoplasmic and nuclear extracts **(e)**. Both extracts were immunoblotted by the indicated

antibodies. **(f)** Plasmids encoding wild-type Flag-Snail1 or Flag-Snail1-3KR were co-transfected with HA-GSK3 $\beta$  into NMuMG cells in the absence or presence of pcDNA-A20. Cell lysates were immunoprecipitated with anti-phospho-serine and anti-Flag antibodies and immunoblotted. **(g)** A20-knockdown or control NMuMG cells were treated with TGF- $\beta$ 1 for 24 h, respectively, and then treated with leptomycin B (5 ng ml $^{-1}$ ) for 4 h. Cells were fractionated into cytoplasmic and nuclear extracts and both extracts were immunoblotted with the indicated antibodies. **(h)** A20-knockdown or control NMuMG cells were treated with TGF- $\beta$ 1. After treatment for 24 h, cells were immunostained with the indicated antibodies. Scale bars, 20  $\mu$ m. All data are representative of three independent experiments. Expression levels of tubulin and lamin **(e,g)** were used as cytoplasmic and nuclear markers and loading controls. In all immunoblot analysis except for **e,g**, expression of  $\beta$ -actin was used as a loading control. Unprocessed original scans of blots in Fig. 7 are shown in Supplementary Fig. 9.

was decreased in stage III TNBC patients, whereas TGF- $\beta$ 1 expression was increased in stage III TNBC patients (Fig. 8i). In addition, A20 expression by TGF- $\beta$ 1 was later induced by a Smad-independent non-canonical pathway (Supplementary Fig. 7b–d).

## DISCUSSION

We here identified a role for A20 in the metastasis of basal-like breast cancers and TGF- $\beta$ -induced EMT. Therefore, our present study strongly proposes a pathway linking the immune regulator A20 to the

EMT-mediated metastatic process. Besides the induction of A20 by TNF- $\alpha$  treatment<sup>10,11</sup>, our results suggest that A20 expression may be upregulated by TGF- $\beta$ 1, crucial in tumour progression. Inflammation is critical in cancer progression<sup>55,56</sup>, and a significant number of immune cells infiltrate into neoplastic tissues, and various cytokines and chemokines, including TNF- $\alpha$  and TGF- $\beta$ 1, are released by both these infiltrated immune cells and cancer cells<sup>57,58</sup>. Our studies indicated that A20 is required for TNF- $\alpha$ - and TGF- $\beta$ 1-induced Snail1 stabilization. Hence, increased levels of TNF- $\alpha$  or TGF- $\beta$ 1 may augment

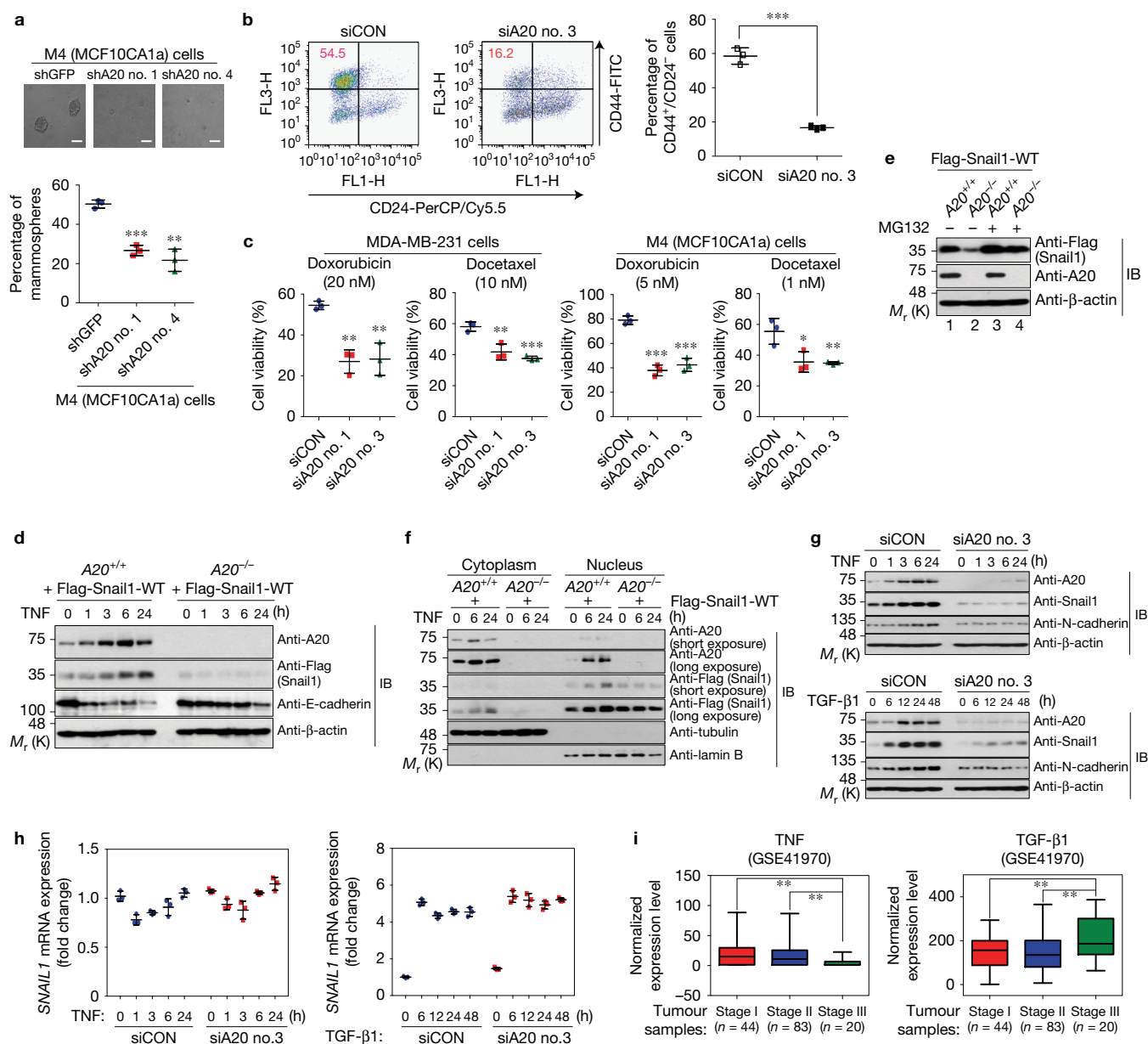


**Figure 8** A20 is required for cancer stemness, chemoresistance, and TNF- $\alpha$ -induced Snail1 stabilization. **(a)** Mammosphere formation of A20-depleted M4 cells. Mammospheres with diameter above 50  $\mu$ m were counted. Scale bars, 50  $\mu$ m. **(b)** FACS analysis of CD44<sup>+</sup>/CD24<sup>-</sup> cancer cells in A20-depleted M4 cells. The proportion of CD44<sup>+</sup>/CD24<sup>-</sup> fraction was described with the density plots and in a bar graph. In **a** and **b**, shGFP or control siRNA was used as a control. **(c)**  $2 \times 10^4$  cells of A20-depleted MDA-MB-231 and M4 were respectively treated with doxorubicin and docetaxel and their viabilities were monitored at 24 h. Data in **a–c** were statistically analysed by a *t*-test and show the mean  $\pm$  s.d. of  $n=3$  independent experiments. \* $P < 0.05$ , \*\* $P < 0.01$  and \*\*\* $P < 0.001$  compared with control cells. **(d)** Immunoblots of Snail1 in A20<sup>+/+</sup> and A20<sup>-/-</sup> MEFs expressing Flag-Snail1 following TNF- $\alpha$  (20 ng ml<sup>-1</sup>) treatment for the indicated time. **(e)** Immunoblots of Snail1 in A20<sup>+/+</sup> and A20<sup>-/-</sup> MEFs expressing Flag-Snail1 with or without MG132. **(f)** Cells were fractionated into cytoplasmic and nuclear extracts.

Both extracts were immunoblotted. **(g,h)** Expression of Snail1 protein **(g)** and SNAIL1 mRNA **(h)** in A20-depleted and control HS578T cells following TNF- $\alpha$  (20 ng ml<sup>-1</sup>) or TGF- $\beta$ 1 (5 ng ml<sup>-1</sup>) treatment. Images in **d–g** are representative of three independent experiments. Data from qRT-PCR analysis **(h)** were statistically analysed by a *t*-test and show the mean  $\pm$  s.d. of  $n=3$  independent experiments. Expression of  $\beta$ -actin was used as a loading control in **d,e** and **g**. Expression levels of tubulin and lamin were used as cytoplasmic and nuclear markers and loading controls **(f)**. **(i)** Expression levels of TNF- $\alpha$  and TGF- $\beta$ 1 mRNAs in different stage TNBC samples (GSE41970,  $n=44$  stage I tumours,  $n=83$  stage II tumours and  $n=20$  stage III tumours). Boxes represent the interquartile range and the centre is the median. The minimum and maximum values are represented by the whiskers. *P* values were calculated by a *t*-test. \*\* $P < 0.01$  compared with stage I or stage II TNBC samples. Source data for **a–c,h** are available in Supplementary Table 3. Unprocessed scans of blots in **d–g** are shown in Supplementary Fig. 9.

A20 induction, subsequently inducing EMT by stabilizing multi-monoubiquitylated Snail1, eventually contributing to the metastasis of breast cancers.

Additionally, the different induction kinetics of A20 in several cell types by TNF- $\alpha$  or TGF- $\beta$ 1 may reflect a distinct role of each cytokine during cancer progression. TNF- $\alpha$ , which is secreted from cancer cells

or infiltrated immune cells at early stages of cancer progression, can increase inflammation-induced EMT of breast cancers through the induction of A20, and at the late stage, cancer cells or other immune cells secrete TGF- $\beta$ 1, resulting in TGF- $\beta$ -induced EMT. This speculation was supported by analysis of the GSE41970 data set<sup>54</sup> (Fig. 8i). However, not all public data sets we analysed reveal a similar correlation. This is probably in part due to the infiltrating immune cells recruited into the tumours of TNBC patients. Although TNF- $\alpha$  and TGF- $\beta$ 1 contribute to the malignant progression of TNBC, their amounts in the tumour microenvironments of different stages of TNBC can be affected by infiltrated immune cells as well as tumour cells. Because expression profiles of mRNAs in public data sets are obtained from tumour samples, they do not fully reflect the profiles of TNF- $\alpha$  and TGF- $\beta$ 1 in a tumour microenvironment. Therefore, further comprehensive work is needed to understand the *in vivo* role of these cytokines in the tumour microenvironments of breast cancer patients.

A20 expression might act as a prognostic biomarker to predict metastasis and survival of breast cancer patients, in addition to Snail1, a known biomarker in breast cancers<sup>41,59</sup>. A role for A20 as a prognostic biomarker was observed in the analysis of relapse-free survival of breast cancer patients of GSE public data sets (GSE9195 and GSE2603) (Supplementary Fig. 8a). Although the increased expression of A20 is apparently related to worse outcomes in breast cancer patients, the correlation between A20 expression and clinical outcomes seems to be specific for breast and pancreatic cancers, which are subject to TGF- $\beta$ 1-induced EMT. Considering that unidentified E3 ubiquitin ligases may be responsible for Snail1 monoubiquitylation in other cancers, it is worth investigating E3 ligase candidates and subsequent Snail1 monoubiquitylation in other malignant tumours.

In conclusion, our results reveal a mechanism regulating the TGF- $\beta$ -mediated EMT process through Snail1 multi-monoubiquitylation, as well as a unique function of A20 in the metastasis of aggressive basal-like breast cancers (Supplementary Fig. 8b). Modulation of the A20–Snail1 axis in TGF- $\beta$ -mediated EMT may be a promising target for therapeutic intervention against the metastasis of aggressive breast cancers. □

## METHODS

Methods, including statements of data availability and any associated accession codes and references, are available in the [online version of this paper](#).

*Note: Supplementary Information is available in the online version of the paper*

## ACKNOWLEDGEMENTS

This work was supported by a grant from the National R&D Program for Cancer Control, Ministry for Health and Welfare, Republic of Korea (1520120) and in part by National Research Foundation grant of Korea (2015R1A2A2A05001344 and SRC 2017R1A5A1014560) funded by the Ministry of Science, ICR & Future Planning.

## AUTHOR CONTRIBUTIONS

J.-H.L. and S.M.J. designed the research, carried out the experimental work, analysed data and wrote the manuscript; E.B., J.S.P. and J.-H.K. performed the animal experiments and immunohistochemical analysis; D.S., M.K., J.H., J.L. and J.H.K. carried out the experimental work and analysed data; K.-M.Y., S.G.A., A.O. and J.J. statistically analysed the public data sets and clinical data of breast cancer patients; J.P., D.S., Y.S.L. and S.L. carried out *in vitro* ubiquitylation and provided technical assistance; G.L. and S.-J.K. participated in the study design and coordinated the study; S.H.P. designed and conceptualized the research, supervised the experimental work, analysed data and wrote the manuscript.

## COMPETING FINANCIAL INTERESTS

The authors declare no competing financial interests.

Published online at <http://dx.doi.org/10.1038/ncb3609>

Reprints and permissions information is available online at [www.nature.com/reprints](http://www.nature.com/reprints)  
 Publisher's note: Springer Nature remains neutral with regard to jurisdictional claims in published maps and institutional affiliations.

- Perou, C. M. *et al.* Molecular portraits of human breast tumours. *Nature* **406**, 747–752 (2000).
- Dent, R. *et al.* Triple-negative breast cancer: clinical features and patterns of recurrence. *Clin. Cancer Res.* **13**, 4429–4434 (2007).
- Hudis, C. A. & Gianni, L. Triple-negative breast cancer: an unmet medical need. *Oncologist* **16**, 1–11 (2011).
- Foulkes, W. D., Smith, I. E. & Reis-Filho, J. S. Triple-negative breast cancer. *N. Engl. J. Med.* **363**, 1938–1948 (2010).
- Lee, E. G. *et al.* Failure to regulate TNF-induced NF- $\kappa$ B and cell death responses in A20-deficient mice. *Science* **289**, 2350–2354 (2000).
- Ma, A. & Malynn, B. A. A20: linking a complex regulator of ubiquitylation to immunity and human disease. *Nat. Rev. Immunol.* **12**, 774–785 (2012).
- Catrysse, L., Vereecke, L., Beyaert, R. & van Loo, G. A20 in inflammation and autoimmunity. *Trends Immunol.* **35**, 22–31 (2014).
- Musone, S. L. *et al.* Multiple polymorphisms in the TNFAIP3 region are independently associated with systemic lupus erythematosus. *Nat. Genet.* **40**, 1062–1064 (2008).
- Adrianto, I. *et al.* Association of a functional variant downstream of TNFAIP3 with systemic lupus erythematosus. *Nat. Genet.* **43**, 253–258 (2011).
- Dixit, V. M. *et al.* Tumor necrosis factor- $\alpha$  induction of novel gene products in human endothelial cells including a macrophage-specific chemotaxin. *J. Biol. Chem.* **265**, 2973–2978 (1990).
- Opipari, A. W. Jr, Boguski, M. S. & Dixit, V. M. The A20 cDNA induced by tumor necrosis factor  $\alpha$  encodes a novel type of zinc finger protein. *J. Biol. Chem.* **265**, 14705–14708 (1990).
- Opipari, A. W. Jr, Hu, H. M., Yabkowitz, R. & Dixit, V. M. The A20 zinc finger protein protects cells from tumor necrosis factor cytotoxicity. *J. Biol. Chem.* **267**, 12424–12427 (1992).
- Beyaert, R., Heynincx, K. & Van Huffel, S. A20 and A20-binding proteins as cellular inhibitors of nuclear factor- $\kappa$ B-dependent gene expression and apoptosis. *Biochem. Pharmacol.* **60**, 1143–1151 (2000).
- Tavares, R. M. *et al.* The ubiquitin modifying enzyme A20 restricts B cell survival and prevents autoimmunity. *Immunity* **33**, 181–191 (2010).
- Vereecke, L. *et al.* Enterocyte-specific A20 deficiency sensitizes to tumor necrosis factor-induced toxicity and experimental colitis. *J. Exp. Med.* **207**, 1513–1523 (2010).
- Kool, M. *et al.* The ubiquitin-editing protein A20 prevents dendritic cell activation, recognition of apoptotic cells, and systemic autoimmunity. *Immunity* **35**, 82–96 (2011).
- Matmati, M. *et al.* A20 (TNFAIP3) deficiency in myeloid cells triggers erosive polyarthritis resembling rheumatoid arthritis. *Nat. Genet.* **43**, 908–912 (2011).
- Hammer, G. E. *et al.* Expression of A20 by dendritic cells preserves immune homeostasis and prevents colitis and spondyloarthritis. *Nat. Immunol.* **12**, 1184–1193 (2011).
- Lippens, S. *et al.* Keratinocyte-specific ablation of the NF- $\kappa$ B regulatory protein A20 (TNFAIP3) reveals a role in the control of epidermal homeostasis. *Cell Death Differ.* **18**, 1845–1853 (2011).
- Vande Walle, L. *et al.* Negative regulation of the NLRP3 inflammasome by A20 protects against arthritis. *Nature* **512**, 69–73 (2014).
- Catrysse, L. *et al.* A20 prevents chronic liver inflammation and cancer by protecting hepatocytes from death. *Cell Death Dis.* **7**, e2250 (2016).
- Boone, D. L. *et al.* The ubiquitin-modifying enzyme A20 is required for termination of Toll-like receptor responses. *Nat. Immunol.* **5**, 1052–1060 (2004).
- Lin, S. C. *et al.* Molecular basis for the unique deubiquitinating activity of the NF- $\kappa$ B inhibitor A20. *J. Mol. Biol.* **376**, 526–540 (2008).
- Komander, D. & Barford, D. Structure of the A20 OTU domain and mechanistic insights into deubiquitination. *Biochem. J.* **409**, 77–85 (2008).
- Wertz, I. E. *et al.* De-ubiquitination and ubiquitin ligase domains of A20 downregulate NF- $\kappa$ B signalling. *Nature* **430**, 694–699 (2004).
- Bosanac, I. *et al.* Ubiquitin binding to A20 ZnF4 is required for modulation of NF- $\kappa$ B signaling. *Mol. Cell* **40**, 548–557 (2010).
- Skaug, B. *et al.* Direct, noncatalytic mechanism of IKK inhibition by A20. *Mol. Cell* **44**, 559–571 (2011).
- Guo, Q. *et al.* A20 is overexpressed in glioma cells and may serve as a potential therapeutic target. *Expert. Opin. Ther. Targets* **13**, 733–741 (2009).
- Hjelmeland, A. B. *et al.* Targeting A20 decreases glioma stem cell survival and tumor growth. *PLoS Biol.* **8**, e1000319 (2010).
- Dong, B. *et al.* Targeting A20 enhances TRAIL-induced apoptosis in hepatocellular carcinoma cells. *Biochem. Biophys. Res. Commun.* **418**, 433–438 (2012).
- Vendrell, J. A. *et al.* A20/TNFAIP3, a new estrogen-regulated gene that confers tamoxifen resistance in breast cancer cells. *Oncogene* **26**, 4656–4667 (2007).
- Chen, S. *et al.* Up-regulated A20 promotes proliferation, regulates cell cycle progression and induces chemotherapy resistance of acute lymphoblastic leukemia cells. *Leuk. Res.* **39**, 976–983 (2015).

33. Hovelmeyer, N. *et al.* A20 deficiency in B cells enhances B-cell proliferation and results in the development of autoantibodies. *Eur. J. Immunol.* **41**, 595–601 (2011).
34. Chu, Y. *et al.* B cells lacking the tumor suppressor TNFAIP3/A20 display impaired differentiation and hyperactivation and cause inflammation and autoimmunity in aged mice. *Blood* **117**, 2227–2236 (2011).
35. Thiery, J. P., Acloque, H., Huang, R. Y. & Nieto, M. A. Epithelial-mesenchymal transitions in development and disease. *Cell* **139**, 871–890 (2009).
36. Lamouille, S., Xu, J. & Derynck, R. Molecular mechanisms of epithelial-mesenchymal transition. *Nat. Rev. Mol. Cell Biol.* **15**, 178–196 (2014).
37. Diaz, V. M., Vinas-Castells, R. & Garcia de Herreros, A. Regulation of the protein stability of EMT transcription factors. *Cell Adhes. Migr.* **8**, 418–428 (2014).
38. Derynck, R., Muthusamy, B. P. & Saetern, K. Y. Signaling pathway cooperation in TGF- $\beta$ -induced epithelial-mesenchymal transition. *Curr. Opin. Cell Biol.* **31**, 56–66 (2014).
39. Chen, J., Imanaka, N. & Griffin, J. D. Hypoxia potentiates Notch signaling in breast cancer leading to decreased E-cadherin expression and increased cell migration and invasion. *Br. J. Cancer* **102**, 351–360 (2010).
40. Kim, C. H. *et al.* Implication of snail in metabolic stress-induced necrosis. *PLoS ONE* **6**, e18000 (2011).
41. Zhou, B. P. *et al.* Dual regulation of Snail by GSK-3 $\beta$ -mediated phosphorylation in control of epithelial-mesenchymal transition. *Nat. Cell Biol.* **6**, 931–940 (2004).
42. Riaz, M. *et al.* miRNA expression profiling of 51 human breast cancer cell lines reveals subtype and driver mutation-specific miRNAs. *Breast Cancer Res.* **15**, R33 (2013).
43. Wang, Y. *et al.* Gene-expression profiles to predict distant metastasis of lymph-node-negative primary breast cancer. *Lancet* **365**, 671–679 (2005).
44. Guaita, S. *et al.* Snail induction of epithelial to mesenchymal transition in tumor cells is accompanied by MUC1 repression and ZEB1 expression. *J. Biol. Chem.* **277**, 39209–39216 (2002).
45. Peinado, H., Quintanilla, M. & Cano, A. Transforming growth factor  $\beta$ -1 induces snail transcription factor in epithelial cell lines: mechanisms for epithelial mesenchymal transitions. *J. Biol. Chem.* **278**, 21113–21123 (2003).
46. Zheng, H. *et al.* PKD1 phosphorylation-dependent degradation of SNAIL by SCF-FBXO11 regulates epithelial-mesenchymal transition and metastasis. *Cancer Cell* **26**, 358–373 (2014).
47. Jung, S. M. *et al.* Smad6 inhibits non-canonical TGF- $\beta$ 1 signalling by recruiting the deubiquitinase A20 to TRAF6. *Nat. Commun.* **4**, 2562 (2013).
48. Zhang, K. *et al.* The collagen receptor discoidin domain receptor 2 stabilizes SNAIL1 to facilitate breast cancer metastasis. *Nat. Cell Biol.* **15**, 677–687 (2013).
49. Eiseler, T. *et al.* Protein kinase D1 mediates anchorage-dependent and -independent growth of tumor cells via the zinc finger transcription factor Snail1. *J. Biol. Chem.* **287**, 32367–32380 (2012).
50. Singh, A. & Settleman, J. EMT, cancer stem cells and drug resistance: an emerging axis of evil in the war on cancer. *Oncogene* **29**, 4741–4751 (2010).
51. Fisher, K. R. *et al.* Epithelial-to-mesenchymal transition is not required for lung metastasis but contributes to chemoresistance. *Nature* **527**, 472–476 (2015).
52. Wu, Y. *et al.* Stabilization of Snail1 by NF- $\kappa$ B is required for inflammation-induced cell migration and invasion. *Cancer Cell* **15**, 416–428 (2009).
53. Hsu, D. S. *et al.* Acetylation of Snail modulates the cytokinome of cancer cells to enhance the recruitment of macrophages. *Cancer Cell* **26**, 534–548 (2014).
54. Cascione, L. *et al.* Integrated microRNA and mRNA signatures associated with survival in triple negative breast cancer. *PLoS ONE* **8**, e55910 (2013).
55. Coussens, L. M. & Werb, Z. Inflammation and cancer. *Nature* **420**, 860–867 (2002).
56. Hanahan, D. & Weinberg, R. A. Hallmarks of cancer: the next generation. *Cell* **144**, 646–674 (2011).
57. Moore, R. J. *et al.* Mice deficient in tumor necrosis factor- $\alpha$  are resistant to skin carcinogenesis. *Nat. Med.* **5**, 828–831 (1999).
58. Massague, J. TGF $\beta$  in cancer. *Cell* **134**, 215–230 (2008).
59. Blanco, M. J. *et al.* Correlation of Snail expression with histological grade and lymph node status in breast carcinomas. *Oncogene* **21**, 3241–3246 (2002).
60. Schneider, C. A., Rasband, W. S. & Eliceiri, K. W. NIH Image to ImageJ: 25 years of image analysis. *Nat. Methods* **9**, 671–675 (2012).

## METHODS

**Cell culture and reagents.** Normal murine mammary gland (NMuMG) cells were purchased from the American Type Culture Collection (ATCC) and maintained in DMEM (GIBCO) with 10% FBS (HyClone) and  $10 \mu\text{g ml}^{-1}$  insulin (Sigma). Both wild-type and A20-knockout mouse embryonic fibroblast cells (MEFs) were previously described<sup>61</sup>. 4T1-Luc mouse breast cancer cells expressing luciferase<sup>62</sup> and human embryonic kidney (HEK293) cells<sup>47</sup> were previously described. Human pancreatic cancer Panc-1 cells were kindly provided by D.-K. Lee (Sungkyunkwan University, Korea)<sup>63</sup>. MEFs, 4T1-Luc, HEK293 and Panc-1 cells were maintained in DMEM with 10% FBS. The human mammary epithelial cell line MCF10A cells were purchased from ATCC and maintained in MEBM (Lonza) supplemented with  $100 \text{ ng ml}^{-1}$  cholera toxin (Sigma) and MEGM SingleQuot (Lonza) except for GA-1000 (gentamycin-amphotericin B mix). The MCF10A-derived breast cancer cell lines MCF10AT, MCF10CA1h and MCF10CA1a<sup>62</sup> were maintained in the following conditions: MCF10AT cells were maintained in DMEM/Ham's F-12 nutrient mixture (GIBCO) with 5% horse serum (GIBCO),  $20 \text{ ng ml}^{-1}$  EGF (Peprotech),  $10 \mu\text{g ml}^{-1}$  insulin,  $0.5 \mu\text{g ml}^{-1}$  hydrocortisone (Sigma),  $100 \text{ ng ml}^{-1}$  cholera toxin. The MCF10CA1h and MCF10CA1a cells were maintained in DMEM/Ham's F-12 nutrient mixture with 5% horse serum. Other human breast cancer cells, as previously described<sup>64,65</sup>, were grown in DMEM (MDA-MB-435, MCF7, HS578T and MDA-MB-231) or RPMI (ZR-75B, ZR-75-1, SK-BR-3, T47D and BT549) with 10% FBS. The cell lines in this study were not found in the database of commonly misidentified cell lines maintained by ICLAC and NCBI Biosample and were routinely tested for mycoplasma contamination by PCR. Human and murine recombinant TGF- $\beta$ 1 and TNF- $\alpha$  were obtained from HumanZyme, and R&D Systems, respectively. Cycloheximide (C4859), LiCl (213233), SB431542 (S4317), doxorubicin (D1515) and docetaxel (O1885) were purchased from Sigma. MG132 (M-1157) was obtained from A.G. Scientific, Leptomycin B (L-6100) was purchased from LC Labs. Ubiquitin isopeptidase inhibitor G5 was purchased from Calbiochem (662125). Company names, catalogue numbers, clone numbers, species and dilution ratios of the antibodies used in this study are described in Supplementary Table 1.

**Animal studies.** All procedures for animal experiments were approved by the CHA Laboratory Animal Research Center (Seongnam, Korea) and the Animal Research Center of Sungkyunkwan University (Suwon, Korea) and performed in a manner compliant with all relevant ethical regulations regarding animal research. Animals were housed in a pathogen-free barrier facility with 12 h light/dark cycles and maintained on standard chow. Human MCF10CA1a (M4) breast cancer cells ( $5 \times 10^5$ ), infected with lentiviruses, were injected orthotopically into 5–6-week-old NOD/SCID female mice to measure tumour growth. For metastasis assays, lentivirus-infected MCF10CA1a cells ( $5 \times 10^5$ ) were injected into female NOD/SCID mice through the tail vein. For simultaneous tumorigenesis and metastasis assays, 4T1-Luc mouse breast cancer cells ( $5 \times 10^4$ ), initially infected with lentiviruses or retroviruses, were orthotopically injected into 6-week-old Balb/c female mice. Monitoring of primary tumour growth and the occurrence of lung metastasis was performed by bioluminescence imaging after intraperitoneal injection of D-luciferin. The intensities of bioluminescence signals were measured using an IVS-200 (Xenogen Corp) and IVIS-Lumina XR (Caliper Life Sciences). After five weeks, mice were euthanized and inspected to check primary tumour growth and the presence of lung metastasis. Primary tumour volume was measured by the formula:  $(\text{length}) \times (\text{width})^2 \times 0.5$ . To quantify lung metastasis, lungs were stained with India ink and metastatic nodules were counted. For tumorigenesis and metastasis analysis, the observer was blinded to which animal of each group was being analysed. In all animal experiments, mice were randomly allocated into each experimental group.

**Plasmids.** Flag-tagged human A20 complementary DNA (cDNA) was previously described<sup>47</sup>. Using Flag-A20 plasmid as a template for PCR with specific primers, A20 cDNA was subcloned into the EcoRI and XhoI sites of the pcDNA3-HA, pcDNA3.1 (Invitrogen) and pGEX-5x-1 (Addgene) vectors, resulting in HA-A20, pcDNA-A20 and GST-A20, respectively. Human Flag-Snail1 and Myc- $\beta$ TrCP1 were kindly provided by C. Y. Choi (Sungkyunkwan University, Korea) and Myc- $\beta$ TrCP1 was subcloned into the EcoRI and XhoI sites of the pcDNA3-HA vector after PCR amplification. Plasmids expressing human HA-GSK3 $\beta$ , wild-type His-ubiquitin (His-Ub) and His-Ub7KR mutant were provided by J. Song (Yonsei University, Korea). In His-Ub7KR, all seven lysine residues were mutated into arginine. Human PKD1 and mouse A20 cDNAs were amplified by PCR from the cDNAs of HEK293 and NMuMG cells, respectively. The amplified fragments were cloned into the EcoRI and XhoI sites of the pcDNA3-HA and XhoI and EcoRI sites of pMSCV-puro (Clontech) vectors, respectively. Flag-Snail1 was subcloned into the XhoI and EcoRI sites of the pMSCV-puro vector. Point mutations of A20 or Snail1 were generated by the QuikChange Mutagenesis kit (Stratagene). Briefly, the A20(C624A/C627A) mutant has two cysteine residues of ZnF4 mutated to alanines and the A20(F770A/G771A) mutant has the phenylalanine and glycine of

ZnF7 replaced by alanines, on the basis of the previous reports<sup>25,27</sup>. Both a tyrosine and phenylalanine of ZnF4 of A20 were mutated into alanines, resulting in the A20(Y614A/F615A) mutant. The A20(4A; Y614A/F615A/F770A/G771A) mutant has four critical amino acids, tyrosine (614) and phenylalanine (615) in ZnF4 as well as phenylalanine (770) and glycine (771) in ZnF7, substituted with alanines. The HA-A20(C103A) mutant with impaired DUB activity was previously described<sup>47</sup>. The Snail1(N-6KR) mutant has all six lysine residues in the Snail1 SNAG and serine-rich domain substituted with arginines, and the Snail1(C-8KR) mutant has a total of eight lysine residues in the Snail1 zinc-finger domains replaced with arginines. The Snail1 mutant (Flag-Snail1(S82A/S104A)) has two serine residues mutated into alanines<sup>48</sup>. The mouse *CDH1* promoter region (–178 to +92 base pairs from the transcription start site) was amplified by PCR from the genomic DNA of NMuMG cells, isolated by G-spin (iNTRON). The amplified PCR fragment was cloned into the XhoI and HindIII sites of the pGL3 basic vector (Promega). PCR-generated portions of all constructs in this study were verified by sequencing. Primer sequences for PCR amplification in this study are described in Supplementary Table 2. The (CAGA)<sub>12</sub>-Luc luciferase reporter plasmid was previously described<sup>47</sup>.

**Construction of small hairpin RNAs and lentiviral, retroviral infection.** The short hairpin RNA (shRNA) sequences targeting endogenous mouse and human A20, mouse *SNAIL1* and mouse *SMDA4* are described in Supplementary Table 2. Specific shRNAs were purchased from Mission-shRNA (Sigma). Lentiviruses expressing each shRNA were produced by a lentiviral packaging system from Invitrogen. To generate retroviruses, HEK293FT cells were transfected with pMSCV-puro retroviral vectors expressing Flag-A20, Flag-Snail1 WT and Flag-Snail1-3KR in combination with the retroviral packaging system (Invitrogen), respectively. The culture media containing virus particles were harvested after 48 h. These culture media were added into target cells and subsequently incubated for 24 h with Polybrene ( $8 \mu\text{g ml}^{-1}$ ). After incubation, the medium was replaced with complete medium. After 1 day, the target cells, infected with recombinant lentiviruses or retroviruses, were trypsinized and subjected to puromycin selection.

**In vivo and in vitro ubiquitylation assays.** To perform *in vivo* ubiquitylation assays, cells were harvested in PBS buffer containing 5 mM N-ethyl maleimide (NEM). Cells were lysed in binding buffer (6 M guanidine HCl, 0.1 M Na<sub>2</sub>HPO<sub>4</sub>, 0.1 M NaH<sub>2</sub>PO<sub>4</sub>, 0.01 M Tris (pH 8.0), 10 mM  $\beta$ -mercaptoethanol, 5 mM NEM, 5 mM imidazole) and incubated with Ni-NTA agarose (Qiagen) at 4 °C for 12 h. Ni-NTA-mediated pulldown assays were performed as described previously<sup>47</sup>. To perform *in vitro* ubiquitylation assays,  $10 \mu\text{l}$  of purified Flag-Snail1 proteins from HEK293 cells were added to a reaction with 100 ng of E1 (UBE1, BML-UW9410, Enzo Lifesciences), 250 ng of E2 (UbcH5a, E2-616, Boston Biochem), 500 ng of bacterially produced GST-fusion proteins (GST-A20 or GST-A20 ZnF7\*) and 5  $\mu\text{g}$  of ubiquitin (U6253, Sigma) in 25  $\mu\text{l}$  of reaction buffer (40 mM Tris (pH 7.6), 50 mM NaCl, 5 mM MgCl<sub>2</sub>, 1 mM dithiothreitol, 2 mM ATP) for 3 h at 37 °C. The reaction was stopped by addition of 4 $\times$  sample buffer and boiling. Immunoblotting was next performed using anti-Flag antibody to detect ubiquitin-conjugated Snail1 proteins.

**Transfection and reporter assay.** Plasmids were transiently transfected into HEK293 or NMuMG cells using PEI (polyethylenimine) or Lipofectamine 2000 (Invitrogen), respectively. siRNAs (Qiagen) were reverse-transfected by using Lipofectamine RNAiMAX (Invitrogen). The siRNA sequences targeting endogenous human and mouse A20 or mouse  $\beta$ -*TrCP1* are described in Supplementary Table 2. To analyse *CDH1-Luc* or (CAGA)<sub>12</sub>-*Luc* activity, cells were treated with TGF- $\beta$ 1 ( $5 \text{ ng ml}^{-1}$ ) for the indicated time. Firefly and *Renilla* luciferase activities were measured by a dual-luciferase reporter assay system (Promega). All experiments were independently repeated at least three times with similar results.

**Immunofluorescence and subcellular fractionation assays.** For immunofluorescence assay, cells were fixed by cold methanol at –20 °C for 7 min, followed by blocking (5% BSA in PBS) at room temperature for 30 min and incubation with primary antibodies at 4 °C for 12 h. Company names, catalogue numbers, dilution ratios of anti-E-cadherin, anti-vimentin, anti-N-cadherin, anti-fibronectin, anti-Snail1, anti-A20 and anti-Flag primary antibodies used in this assay are described in Supplementary Table 1. After washing with PBS five times, coverslips were stained with the following secondary antibodies at room temperature for 2 h: Alexa Fluor-488-conjugated goat anti-mouse IgG (Invitrogen, 1:400 for anti-E-cadherin, 1:2000 for anti-Flag), Alexa Fluor-594-conjugated donkey anti-mouse IgG (Invitrogen, 1:200 for anti-N-cadherin, anti-fibronectin and anti-Snail1, 1:400 for anti-E-cadherin) and Alexa Fluor-488-conjugated goat anti-rabbit IgG (Invitrogen, 1:200 for anti-A20, 1:400 for anti-vimentin). Coverslips were stained with DAPI (Sigma) and mounted on glass slides. Cells were examined with a laser-scanning confocal microscope (Carl-Zeiss). The Subcellular Protein Fractionation Kit for Cultured Cells (Thermo Scientific, cat. no. 78840) was used for subcellular fractionations.

**Immunoblot analysis and immunoprecipitation.** For immunoblot analysis, cells were harvested in cold PBS and lysed in lysis buffer (1% Triton X-100, 20 mM Hepes at pH 7.4, 150 mM NaCl, 12.5 mM  $\beta$ -glycerol phosphate, 1.5 mM  $MgCl_2$ , 10 mM NaF, 2 mM dithiothreitol, 1 mM NaOV, 2 mM EGTA, 1 mM phenylmethylsulfonyl fluoride, protein inhibitor cocktail). For immunoblot analysis of surgically dissect cancer samples, tissues were homogenized and lysed in RIPA buffer (150 mM NaCl, 50 mM Tris-HCl at pH 7.5, 0.1% SDS, 1% Triton X-100, 2 mM EDTA, 0.5% Na-deoxycholate) containing protein inhibitor cocktail. After elution by 4 $\times$  sample buffer, protein extracts were boiled, separated by SDS-PAGE, transferred to polyvinylidene difluoride (PVDF) membrane filter and subjected to immunoblot analysis. For immunoprecipitation, cell extracts were incubated with appropriate antibodies and protein G agarose beads (Genedepot) at 4 °C for 12 h. Immuno-complexes were washed twice with lysis buffer, eluted from the beads by 2 $\times$  sample buffer and boiled. Immunoblot analysis was subsequently performed using the indicated antibodies.

**RNA extraction and real-time qRT-PCR.** Total RNA was isolated using the TRIzol reagent (Invitrogen). cDNA synthesis was performed using PrimeScript Reverse Transcriptase (TaKaRa). For real-time qRT-PCR, primer sequences used for the *A20*, *SNAIL1*, *CDH1*, *CDH2*, *VIM*, *PAI-1*, *Smad7* and *Gapdh* genes are described in Supplementary Table 2. Real-time qRT-PCR was performed using an iCycler real-time PCR machine and iQ SYBR Green Supermix (Bio-Rad) to measure the expression of genes under the following conditions: 40 cycles of 95 °C for 30 s, 60 °C for 30 s, and 72 °C for 30 s. All reactions were independently repeated at least three times to ensure reproducibility.

**Cell invasion, migration and proliferation assay.** Cells were harvested and resuspended into serum-free medium. The migration assay was performed with Transwells (Corning Costar), according to the manufacturer's protocol. For the invasion assay, Matrigel invasion chambers were prepared by coating the upper chamber surface with Matrigel (BD Biosciences) at 37 °C for 12 h in a 5% CO<sub>2</sub> incubator. MCF10CA1a (M4) cells (1  $\times$  10<sup>4</sup>) and 4T1-Luc cells (2  $\times$  10<sup>4</sup>) were plated onto the upper chamber containing culture media with 0.1% FBS. The bottom chamber contained culture media with 10% FBS. After 48 h for MCF10CA1a (M4) cells and 24 h for 4T1-Luc cells, non-invasive cells in the upper chamber were removed by a cotton swab. Cells that migrated through the Matrigel and the membrane were fixed with methanol and stained with haematoxylin. Cells were counted in three predetermined fields for quantification. For cell proliferation analysis, cells were plated in 6-well plates on day 0. After the indicated time, cells were trypsinized, resuspended in media and counted with a haemocytometer. All experiments were performed at least three times to ensure reproducibility.

**Human breast cancer tissue microarray and immunohistochemistry.** Tumour tissues from specimens of surgically dissected breast carcinoma were collected at the Gangnam Severance Hospital, Yonsei University College of Medicine (Seoul, Korea) between January 1996 and December 2004 after approval by the institutional review board (IRB approval number 3-2013-0268) in compliance with all relevant ethical regulations regarding research involving human participants. Among these samples, cases presenting an invasive focus by review of archival H&E-stained slides were used to construct tissue microarray (TMA) blocks. Two hundred and fifty-six patients with invasive breast carcinoma were finally enrolled. All volunteers officially gave informed consent for this study. For immunohistochemistry, each TMA slide was stained with rabbit monoclonal anti-A20 antibody (ab92324, Abcam, 1:200) and counterstained with haematoxylin. After staining, slides were scored under a microscope and the correlation between A20 expression level and clinical outcomes was analysed together with A20 expression depending on breast cancer subtypes.

**RNA sequencing.** Total RNAs of each cell were isolated using the TRIzol reagent for RNA sequencing following the manufacturer's instructions. The total RNAs were treated with DNase I, purified with the miRNeasy Mini Kit (Qiagen) and their qualities were checked using an Agilent 2100 Bioanalyzer (Agilent). An Illumina platform (Illumina) was used to analyse transcriptomes with a 90 bp paired-end library. Samples were paired-end sequenced with the IlluminaHiSeq 2000 using HiSeq Sequencing kits.

**Chromatin immunoprecipitation (ChIP).** Cells were crosslinked with 1% formaldehyde and lysed with SDS lysis buffer (1% SDS, 10 mM EDTA, 50 mM Tris at pH 8.1 and protease inhibitor cocktail). Cell lysates were sonicated on wet ice and centrifuged to obtain the sheared DNA-protein complexes. DNA-protein complexes were incubated for 12 h at 4 °C with mouse anti-Flag antibody (F1804,

Sigma) and incubated with Protein A/G agarose beads (sc-2003, Santa Cruz) for 1 h at 4 °C. Immunoprecipitated material was washed according to standard procedures (Upstate protocol). After washing, DNA-protein complexes were eluted with 1% SDS, 100 mM NaHCO<sub>3</sub> and reverse-crosslinked with 200 mM NaCl at 65 °C for 12 h. Next, RNAs and proteins were removed by treating RNase A (iNtRON) and Proteinase K (TaKaRa) and DNAs were purified by purification kit (iNtRON). Purified DNAs were amplified and analysed by PCR or qPCR. Primer sequences for ChIP assay in this study were described in Supplementary Table 2.

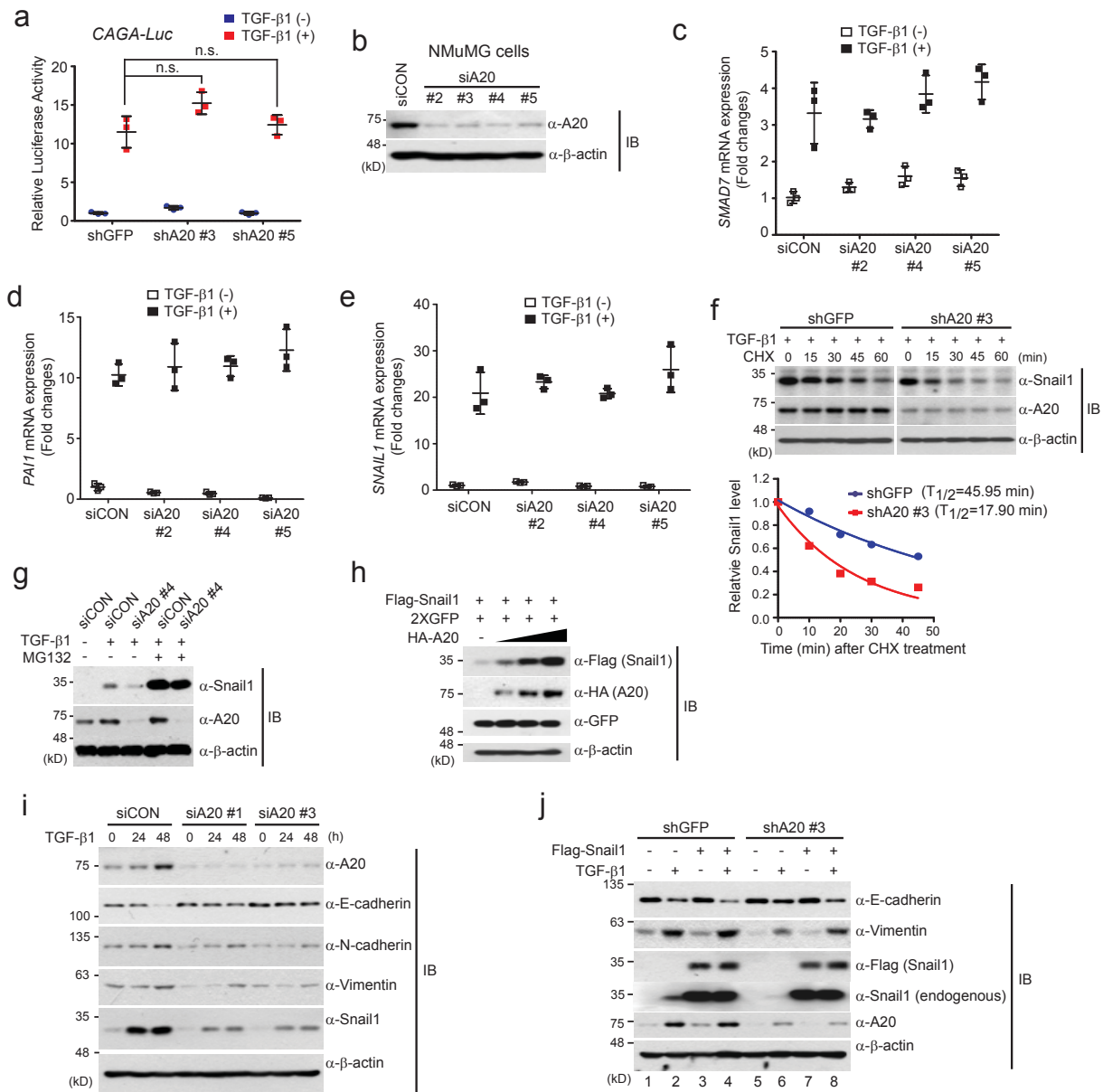
**Mammosphere formation and FACS analysis.** Mammosphere formation assay was performed as described previously<sup>62</sup>. MCF10CA1a cells (1,000 cells per well) were seeded in 96-well ultralow-attachment plates (Corning, 3474) and grown for 5 days in serum-free medium with B27 (Gibco, 17504-044), 20 ng ml<sup>-1</sup> hEGF, 20 ng ml<sup>-1</sup> hFGF (Invitrogen). Mammospheres with diameters above 50  $\mu$ m were counted. For FACS analysis, dissociated single cells were subjected to fluorescence-activated cell sorting (FACS) analysis using cell surface markers for CD44 (eBioscience, 11-0441-81) and CD24 (BioLegend, 101823). The proportion of CD44-positive (+) and CD24-negative (-) population was measured by FACS analysis using FACSCanto II (BD Biosciences) and data were analysed by FlowJo 7.6.5 software.

**Cytotoxicity assay.** Cells were cultured in 96-well plates. After incubation for 36 h, cells were treated with doxorubicin (20 nM for MDA-MB-231 cells, 5 nM for M4 cells) and docetaxel (10 nM for MDA-MB-231 cells, 1 nM for M4 cells) for 12 h. At the end of the treatment, MTT reagent was added to each well and cells were incubated for 20 min at 37 °C in the dark. After supernatants were aspirated, DMSO was added into each well. The absorbance at a wavelength of 550 nm was finally measured using an VersaMax ELISA microplate reader.

**Statistics and reproducibility.** Quantitative data in this study are presented as means  $\pm$  s.d. and were analysed by a two-tailed unpaired Student's *t*-test to compare the difference between groups. *P* < 0.05 was considered statistically significant. The Kaplan-Meier (KM) Plotter Tool (<http://kmplot.com/analysis>)<sup>66</sup> was used to show correlation between A20 expression and the relapse-free survival rates of breast cancer patients. Statistical significance was calculated by a log-rank test. For quantification of protein stability following treatment of cycloheximide, Snail1 and  $\beta$ -actin proteins detected by immunoblotting were quantified using ImageJ software<sup>60</sup>. For normalization,  $\beta$ -actin expression was used as a control. GraphPad Prism 5 and SPSS version 18 software were used in this study. All experiments were repeated at least three times. RNA sequencing using breast cancer cell lines was performed one time. *N* numbers of immunohistochemical analysis and public data set analysis are indicated in the figure legends. Animal studies were performed with adequate *n* numbers to ensure statistical evaluation. No statistical method was used to predetermine sample size. Sample size was chosen on the basis of literature in the field.

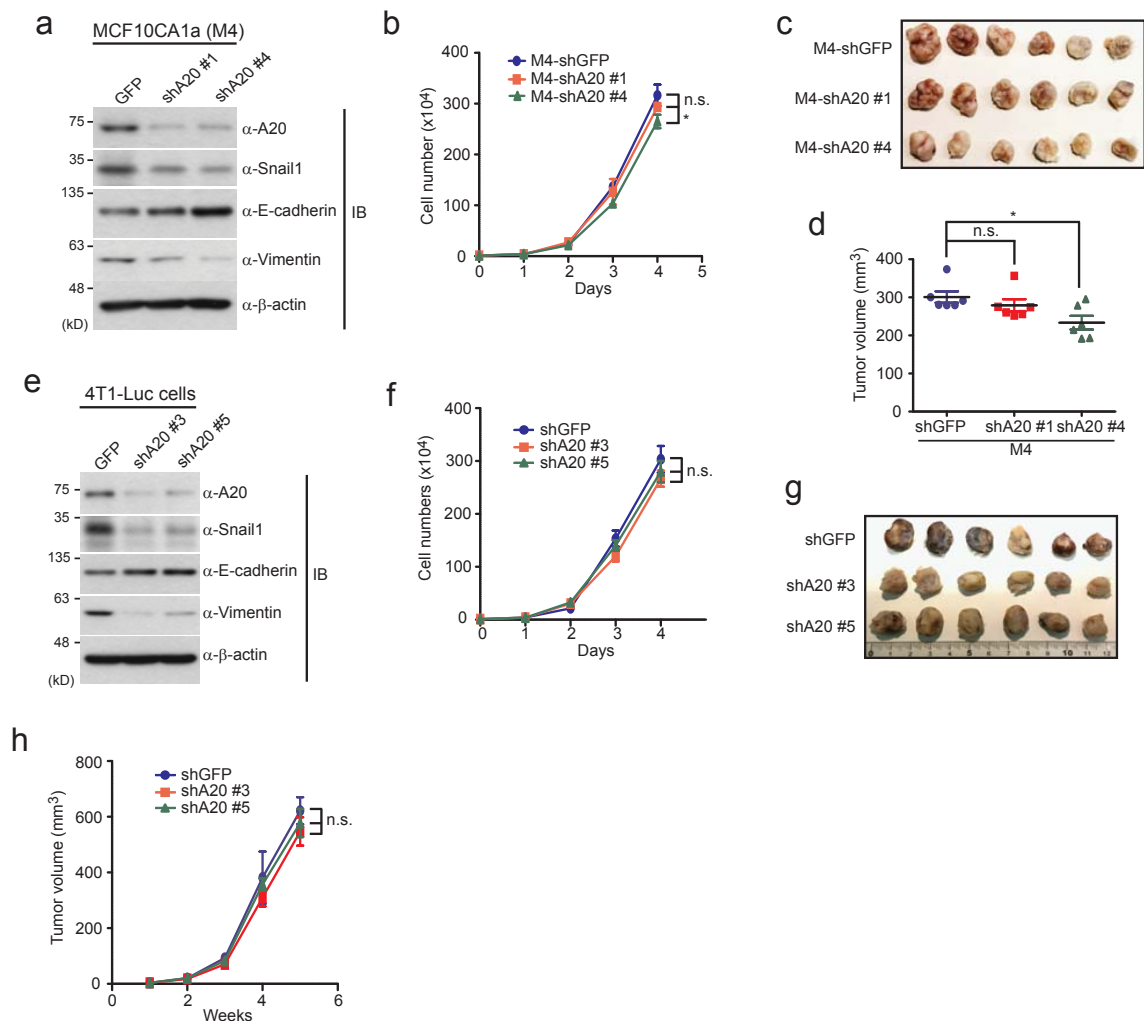
**Data availability.** RNA-sequencing data that support the finding of this study have been deposited in the Gene Expression Omnibus (GEO) under accession code GSE100878. Previously deposited microarray data that were re-analysed here are available under access codes GSE41313 (ref. 42), GSE2034 (ref. 43), GSE41970 (ref. 54), GSE9195 and GSE2603. The microarray data (AgilentG4502A\_07) from 314 tumour (breast invasive carcinoma) and 121 normal samples (normal breast tissue) and RNA-Seq data (IlluminaHiSeq) from 561 tumour (breast invasive carcinoma) and 225 normal samples (normal breast tissue) were downloaded from the TCGA Data Portal (<https://portal.gdc.cancer.gov>). The source data for Figs 2f-i, 3c,e, 4a-c,e,h, 6h and 8a-c,h and Supplementary Figs 1a,c-e and 2b,d,f,h, 4f, 5c,f,h, 6g and 7d have been provided as Supplementary Table 3.

- Verecke, L. *et al.* Enterocyte-specific A20 deficiency sensitizes to tumor necrosis factor-induced toxicity and experimental colitis. *J. Exp. Med.* **207**, 1513-1523 (2010).
- Bae, E. *et al.* Definition of smad3 phosphorylation events that affect malignant and metastatic behaviors in breast cancer cells. *Cancer Res.* **74**, 6139-6149 (2014).
- Dua, P. *et al.* Alkaline phosphatase ALPPL-2 is a novel pancreatic carcinoma-associated protein. *Cancer Res.* **73**, 1934-1945 (2013).
- Yang, K. M. *et al.* Loss of TBK1 induces epithelial-mesenchymal transition in the breast cancer cells by ER $\alpha$  downregulation. *Cancer Res.* **73**, 6679-6689 (2013).
- Kim, M. S. *et al.* Dysregulated JAK2 expression by TrkC promotes metastasis potential, and EMT program of metastatic breast cancer. *Sci. Rep.* **6**, 33899 (2016).
- Gyorffy, B., Surowiak, P., Budczies, J. & Lanczky, A. Online survival analysis software to assess the prognostic value of biomarkers using transcriptomic data in non-small-cell lung cancer. *PLoS ONE* **8**, e82241 (2013).



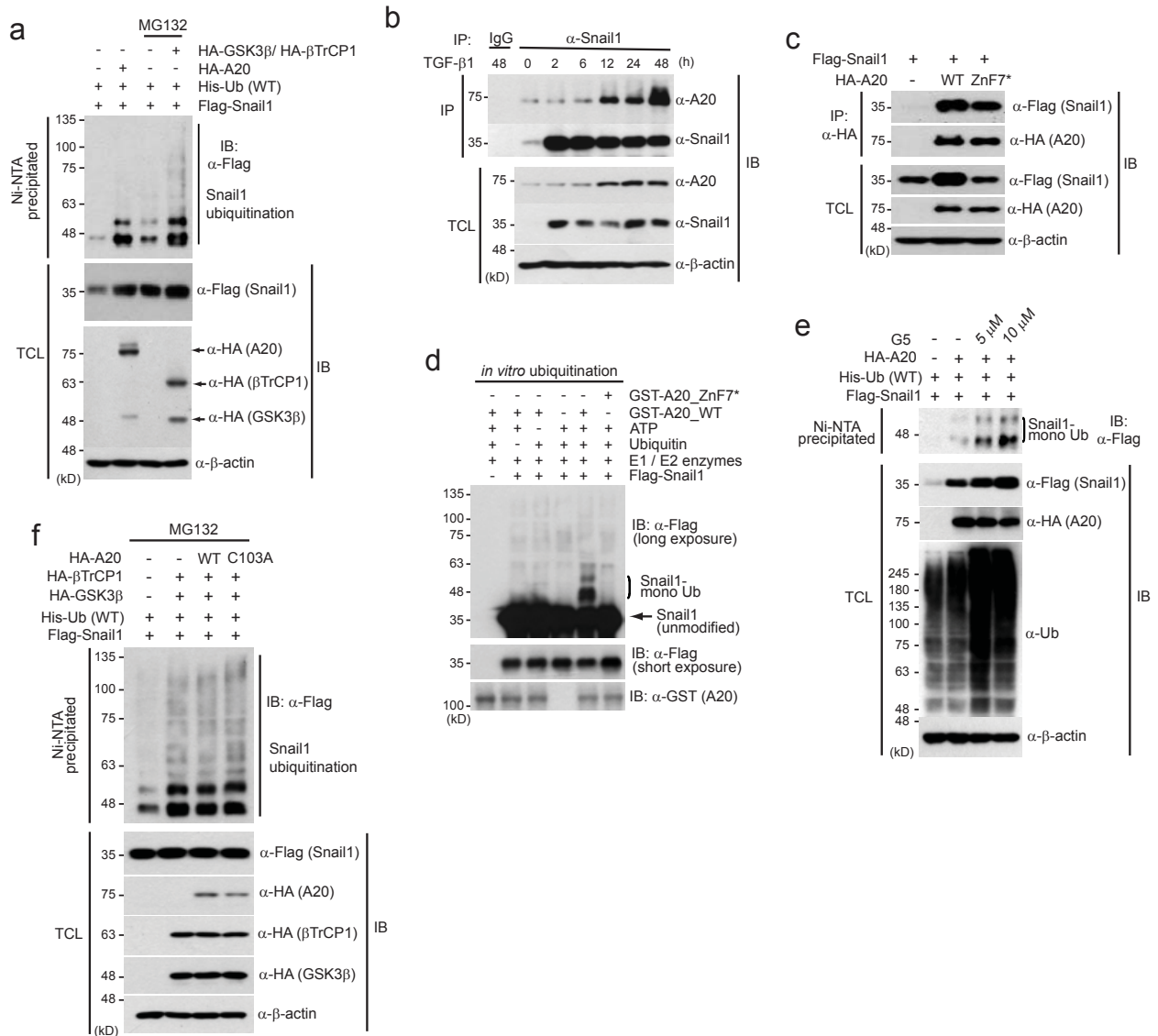
**Supplementary Figure 1** A20 does not affect the canonical TGF- $\beta$ /Smad signaling, but stabilizes the Snail1 protein. **a**, A20-knockdown and shGFP-expressing NMuMG cells were transfected with a Smad-specific *CAGA-Luc* reporter. Cells were treated with TGF- $\beta$ 1 (5 ng/ml) for 24 h, and luciferase activities were measured and normalized. n.s., not significant. **b**, NMuMG cells were reverse-transfected with 20 nM of control siRNA (siCON) or four different siRNAs targeting mouse *A20* mRNA. Knockdown efficiency was confirmed by immunoblot analysis with anti-A20 antibody. **c-e**, Quantitative real-time RT-PCR analysis of indicated target genes, induced by the TGF- $\beta$ /Smad-dependent signaling pathway, in A20-knockdown NMuMG cells treated with TGF- $\beta$ 1 for 24 h. The data in (**a**, **c**, **d**, and **e**) were statistically analyzed by a *t*-test and show the mean  $\pm$  s.d. of  $n=3$  independent experiments. **f**, Stability of the Snail1 protein was measured in A20-knockdown and shGFP-expressing control NMuMG cells in the presence of TGF- $\beta$ 1, followed by treatment of protein translation inhibitor, cycloheximide (CHX, 50  $\mu$ g/ml) for the indicated times. Cell lysates were immunoblotted by the indicated antibodies (upper).

Data were quantified using ImageJ software (lower). For normalization, expression of  $\beta$ -actin was used as a control. **g**, A20-knockdown NMuMG cells were treated with TGF- $\beta$ 1 for 24 h, followed by exposure to proteasomal inhibitor MG132 (10  $\mu$ M) for 6 h. Cell lysates were immunoblotted with the indicated antibodies. **h**, A plasmid encoding Flag-Snail1 was co-transfected with increasing amounts of HA-A20 plasmid into HEK293 cells. Cell lysates were immunoblotted. **i**, Panc-1 cells were reverse-transfected with 20 nM of control siRNA or two independent A20 siRNAs (siA20 #1 and siA20 #3) and treated with TGF- $\beta$ 1 for the indicated times. Cell lysates were immunoblotted. **j**, A20-knockdown and shGFP-expressing control NMuMG cells were transfected with Flag-Snail1 and then treated with TGF- $\beta$ 1 for 24 h. Cell lysates were immunoblotted. Expression of  $\beta$ -actin was used as a loading control for all immunoblot analysis shown in this figure. Immunoblot images are representative of  $n=3$  independent experiments. Statistics source data for (**a**) and (**c**)-(e) are available in Supplementary Table 3. Unprocessed original scans of blots in (**b**) and (**f**)-(j) are in Supplementary Fig. 9.



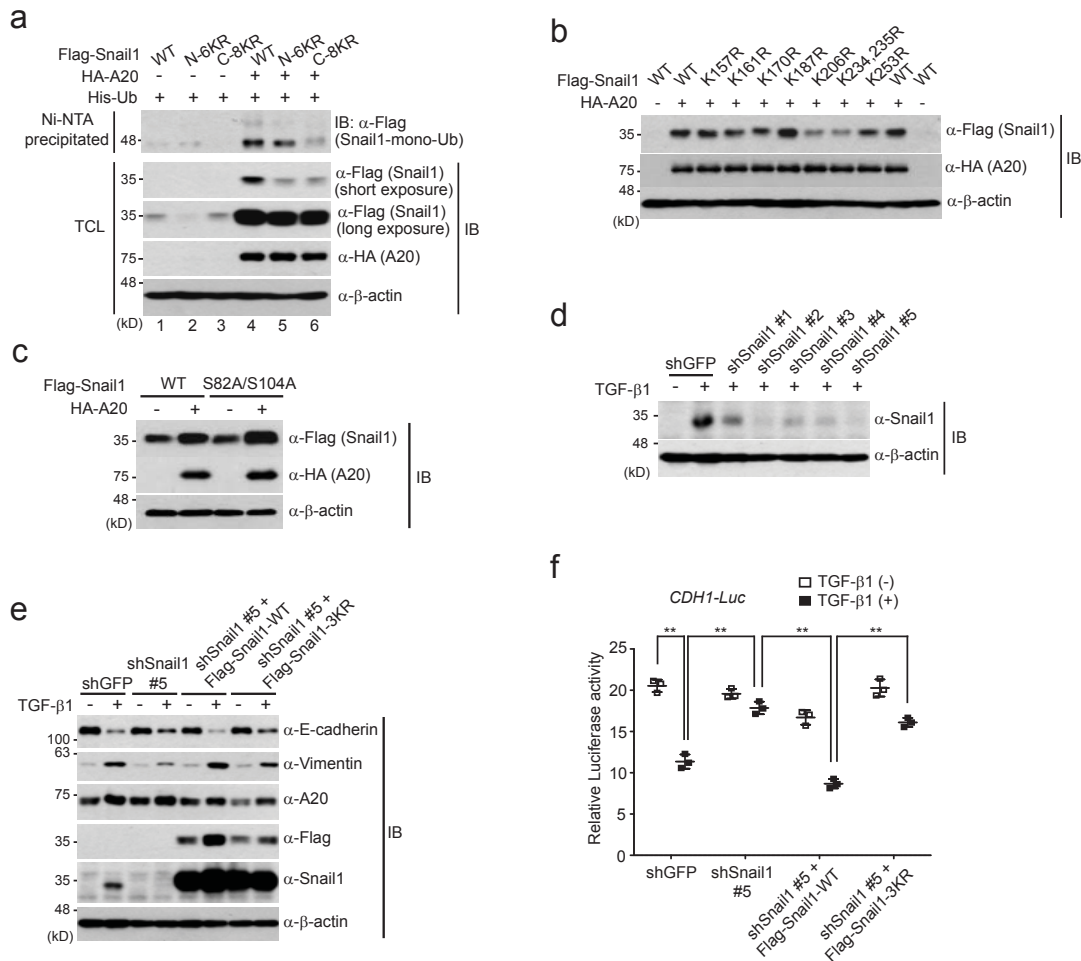
**Supplementary Figure 2** A20 depletion does not affect tumor growth. **a, e**, MCF10CA1a (M4) (**a**) and 4T1-Luc (**e**) cells were infected with the indicated lentiviruses expressing shRNAs targeting A20 mRNA. Cell lysates were immunoblotted with the indicated antibodies. Expression of β-actin was used as a loading control. The data are representative of  $n=3$  independent experiments. **b, f**, A20-knockdown MCF10CA1a (M4) (**b**) or A20-knockdown 4T1-Luc (**f**) cells were cultured in 6-well plates and harvested at the indicated time points. Cell proliferation was analyzed by counting cell numbers in each well, compared to shGFP-expressing control cells. The data were statistically analyzed by a *t*-test and show the mean  $\pm$  s.d. of  $n=3$  independent experiments. \* $P < 0.05$  compared to the shGFP control cells. n.s., not significant. **c, d**,  $5 \times 10^5$  of A20-knockdown and shGFP-expressing

MCF10CA1a (M4) cells were orthotopically injected into NOD/SCID mice ( $n=6$  mice per group). After the mice were sacrificed 5 weeks later, representative primary tumor images were shown in (**c**) and tumor volumes were measured (**d**). **g, h**,  $5 \times 10^4$  of A20-knockdown and shGFP-expressing control 4T1-Luc cells were orthotopically injected into Balb/c mice ( $n=6$  mice per group) and the mice were sacrificed 5 weeks later. Representative images of primary tumors were shown in (**g**) and tumor volumes were measured (**h**). The data in (**d** and **h**) were statistically analyzed by a *t*-test and show the mean  $\pm$  s.d.  $n=6$  mice per group per experiment. \* $P < 0.05$  compared to the shGFP control cells. n.s., not significant. Statistics source data for (**b**), (**d**), (**f**) and (**h**) are available in Supplementary Table 3. Unprocessed original scans of blots in (**a**) and (**e**) are in Supplementary Fig. 9.



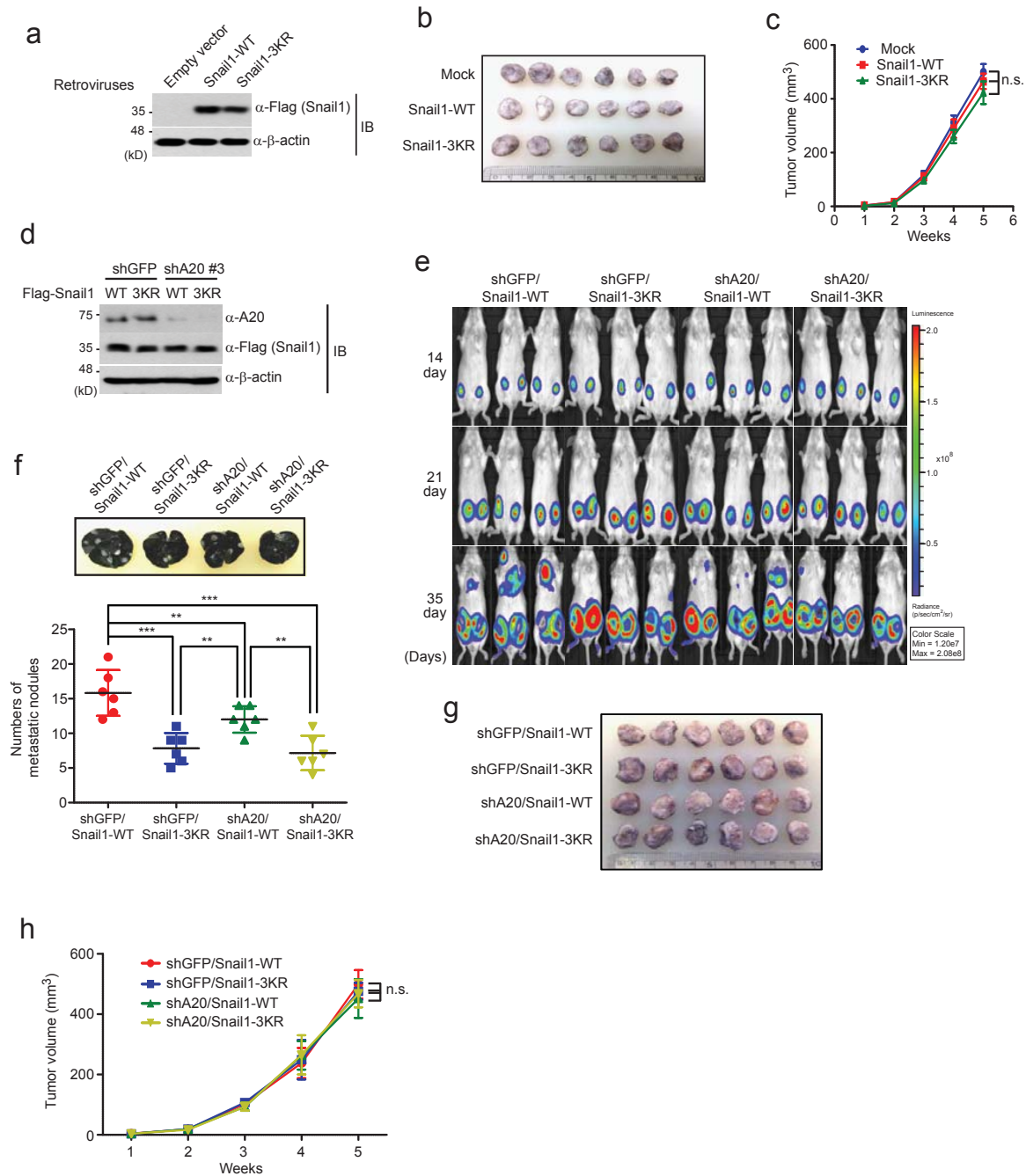
**Supplementary Figure 3** A20 induces monoubiquitination of the Snail1 protein through ZnF7 domain. **a**, Plasmids encoding Flag-Snail1 and wild type His-Ub were co-transfected with HA-A20, HA-GSK3β and HA-βTrCP1 into NMuMG cells in the indicated combinations. Ni-NTA-mediated pull-down assays were performed and ubiquitinated Snail1 was observed by immunoblotting using anti-Flag antibody. Total cell lysates (TCL) were immunoblotted with the indicated antibodies. **b**, Dynamics of the interaction between endogenous A20 and Snail1 in NMuMG cells. Cells were treated with TGF-β1 (5 ng/ml) for the indicated times, immunoprecipitated with anti-Snail1 antibody and immunoblotted with the indicated antibodies. **c**, Plasmid encoding wild-type HA-A20 or A20 ZnF7 mutant (HA-A20\_ZnF7\*) was co-transfected into HEK293 cells together with Flag-Snail1 plasmid. Cell lysates were immunoprecipitated with anti-HA antibody and subsequently immunoblotted with the indicated antibodies. **d**, For *in vitro* ubiquitination assays, Flag-Snail1 proteins were eluted from HEK293 cells

transfected with Flag-Snail1 plasmid, and wild-type GST-A20 and mutant GST-A20\_ZnF7\* proteins were purified from *E. coli*. The reactions were performed in the indicated combinations and samples were immunoblotted with the indicated antibodies. **e**, Plasmids encoding Flag-Snail1 and wild type His-Ub were co-transfected into NMuMG cells with HA-A20. After cells were treated with the ubiquitin isopeptidase inhibitor G5 for 6 h, Ni-NTA pull-down assays were performed, followed by immunoblotting with the indicated antibodies. **f**, Plasmid encoding HA-A20 or HA-A20(C103A) mutant was co-transfected into NMuMG cells with HA-GSK3β and HA-βTrCP1 in the presence of His-Ub and Flag-Snail1. After cells were pre-treated with MG132, Ni-NTA pull-down and immunoblot assays were performed. Expression of β-actin was used as a loading control in all immunoblot assays except for **(d)**. Immunoblot images in this figure are representative of *n*=3 independent experiments. Unprocessed original scans of blots in Supplementary Fig. 3 are in Supplementary Fig. 9.



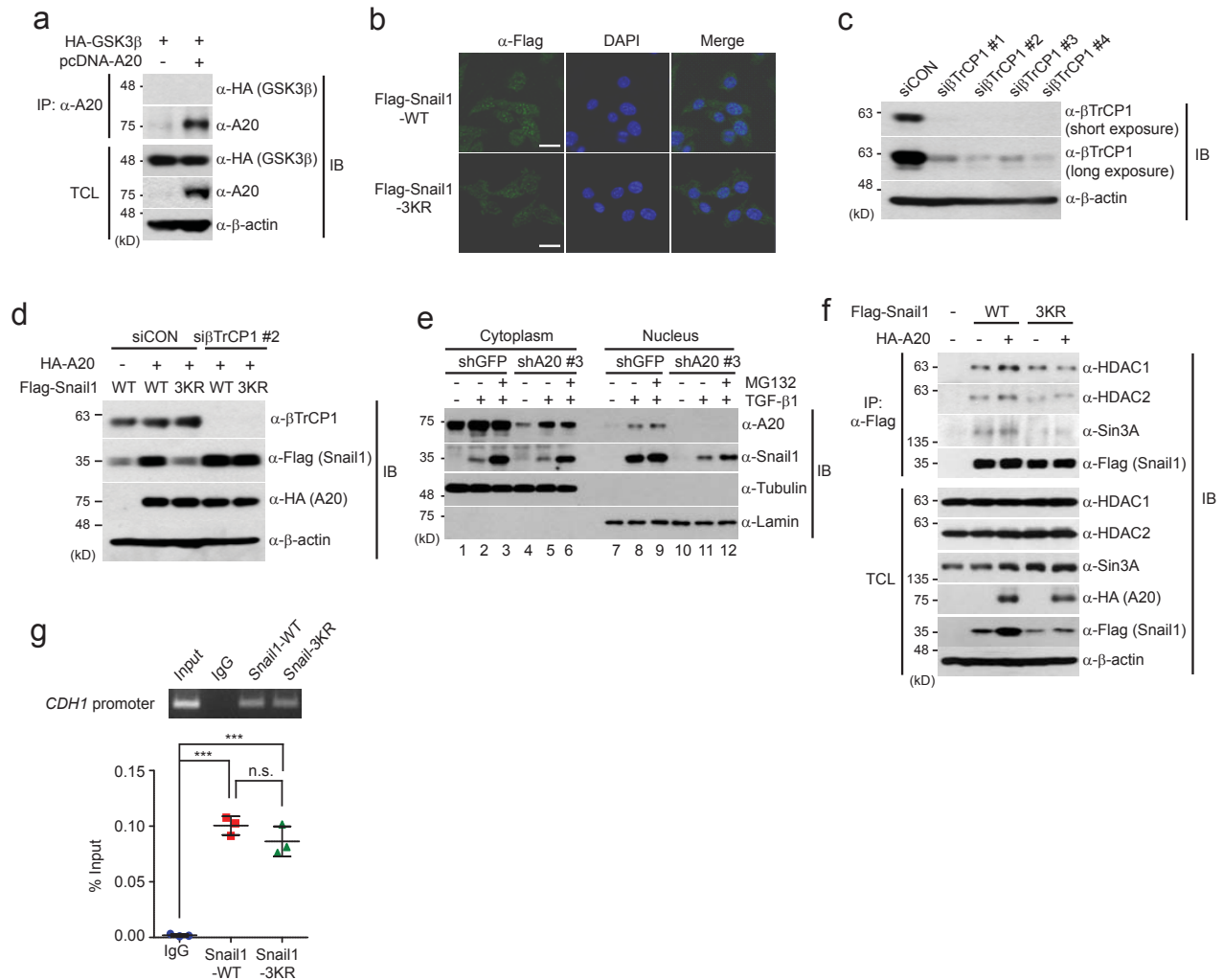
**Supplementary Figure 4** A20 monoubiquitinates three Snail1 lysine residues, which are crucial for Snail1 stability and TGF-β1-induced EMT. **a**, Plasmids encoding wild type Snail1(Flag-Snail1-WT) or Snail1 mutants (Flag-Snail1-N-6KR and Flag-Snail1-C-8KR) were co-transfected into NMuMG cells with wild-type His-Ub and HA-A20 plasmids in the indicated combinations. Ni-NTA-mediated pull-down assays were performed and ubiquitinated Snail1 was observed by immunoblot analysis using anti-Flag antibody. Total cell lysates (TCL) were immunoblotted with the indicated antibodies. **b**, A plasmid encoding wild-type Snail1 (Flag-Snail1) or single K-to-R mutants of Snail1 was co-transfected into NMuMG cells in the absence or presence of HA-A20. Cell lysates were immunoblotted with the indicated antibodies. **c**, To examine whether A20-mediated monoubiquitination of Snail1 is linked to the phosphorylation of Snail1 by ERK, a plasmid encoding a Snail1 mutant [Flag-Snail1(S82A/S104A)] or wild-type Snail1, was co-transfected into NMuMG cells with or without HA-A20. Cell lysates were immunoblotted with the indicated antibodies.

**d**, Snail1 depletion in NMuMG cells by lentiviruses expressing different shRNAs was confirmed by immunoblot analysis with anti-Snail1 antibody. **e**, Snail1-depleted NMuMG cells were infected with retroviruses expressing wild-type Snail1 (Flag-Snail1-WT) or the Snail1(3KR) mutant (Flag-Snail1-3KR). After treatment with TGF-β1 (5 ng/ml) for 48 h to induce EMT, cell lysates were immunoblotted with the indicated antibodies. **f**, The *CDH1-Luc* reporter plasmid was co-transfected into Snail1-depleted NMuMG cells with an indicated plasmid. After treatment with TGF-β1 for 48 h, luciferase activities were measured and normalized. The data were statistically analyzed by a *t*-test and show the mean ± s.d. of *n*=3 independent experiments. \*\**P* < 0.01 compared to cells not treated with TGF-β1 in the case of shGFP and compared to cells treated with TGF-β1 in others. Immunoblot images in this figure are representative of *n*=3 independent experiments and expression of β-actin was used as a loading control. Statistics source data for (f) are available in Supplementary Table 3. Unprocessed original scans of blots in (a)-(e) are in Supplementary Fig. 9.



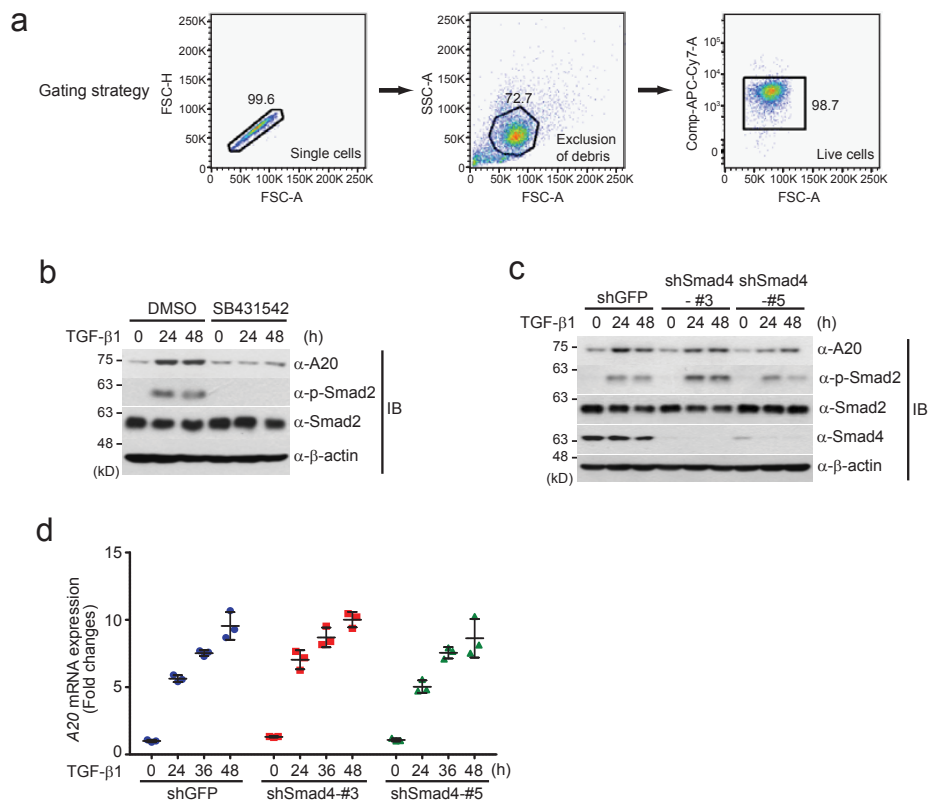
**Supplementary Figure 5** Three lysine residues of Snail1 are essential for breast cancer metastasis. **a**, 4T1-Luc cells stably expressing wild-type Snail1 (Flag-Snail1-WT) or the Snail1(3KR) mutant (Flag-Snail1-3KR) were generated by infection with recombinant retroviruses. Expression of Flag-Snail1-WT or Flag-Snail1-3KR in 4T1-Luc cells were confirmed by immunoblot analysis with anti-Flag antibody. **b, c**,  $5 \times 10^4$  of 4T1-Luc cells stably expressing Flag-Snail1-WT or Flag-Snail1-3KR were orthotopically injected into Balb/c mice ( $n=6$  mice per group). As a control, the same amounts of 4T1-Luc cells infected with retroviruses expressing empty vector (Mock) were used. After the mice were sacrificed 5 weeks later, representative images of primary tumors (**b**) were shown and tumor volumes (**c**) were measured. The data in (**c**) were statistically analyzed by a *t*-test and show the mean  $\pm$  s.d., compared to control 4T1-Luc cells (Mock).  $n=6$  mice per group per experiment. n.s., not significant. **d**, Generation of recombinant 4T1-Luc cell lines expressing Flag-Snail1-WT or Flag-Snail1-

3KR in A20-depleted and shGFP background by consecutive retroviral and lentiviral infections. A20 depletion and Snail1 expression were confirmed by immunoblot analysis. **e-h**, Each recombinant 4T1-Luc cell line ( $5 \times 10^4$  cells) was orthotopically injected into Balb/c mice ( $n=6$  mice per group). Bioluminescence imaging was monitored at the indicated time points (**e**). After the mice were sacrificed 35 days later, lungs were removed and stained with India ink. Representative images and the numbers of metastatic nodules (**f**), images of primary tumors (**g**) and tumor volumes (**h**) were shown. The data in (**f** and **h**) were statistically analyzed by a *t*-test and show the mean  $\pm$  s.d.  $n=6$  mice per group per experiment.  $**P < 0.01$  and  $***P < 0.001$  compared to the indicated groups. n.s.; not significant. Immunoblot images in (**a** and **d**) are representative of  $n=3$  independent experiments and expression of  $\beta$ -actin was used as a loading control. Statistics source data for (**c**), (**f**), and (**h**) are available in Supplementary Table 3. Unprocessed original scans of blots in (**a**), and (**d**) are in Supplementary Fig. 9.



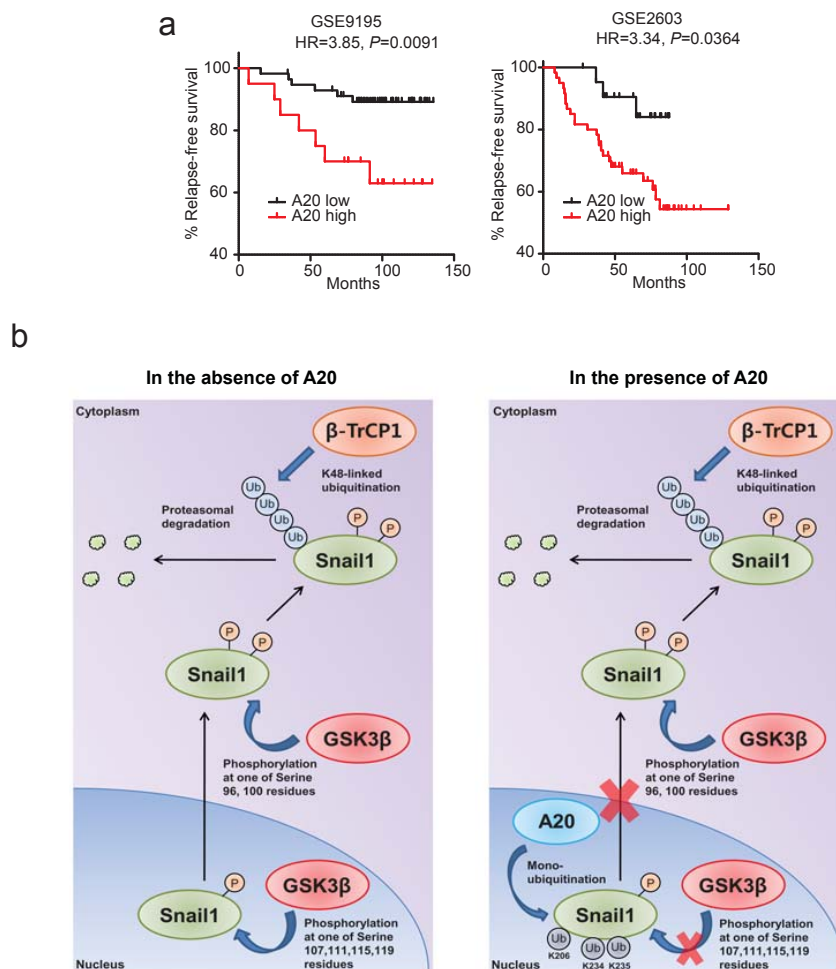
**Supplementary Figure 6** A20-mediated Snail1 monoubiquitination is required for nuclear retention of Snail1 and interaction with transcriptional co-repressors. **a**, A plasmid encoding HA-GSK3β was transfected into HEK293 cells with or without A20 expression plasmid. Cell lysates were immunoprecipitated with anti-A20 antibody and subsequently immunoblotted. **b**, NMuMG cells were infected with retroviruses expressing wild-type Snail1 (Flag-Snail1-WT) or the Snail1(3KR) mutant (Flag-Snail1-3KR). After cells were stained with anti-Flag antibody and DAPI, the localization of Snail1 protein was observed by confocal microscopy. Scale bars, 20 μm. **c**, β-TrCP1 depletion in NMuMG cells by different siRNAs targeting β-TrCP1 mRNA or control siRNA (siCON) was confirmed by immunoblot analysis with anti-β-TrCP1 antibody. **d**, β-TrCP1-depleted (siβTrCP1 #2) NMuMG cells were transfected with a plasmid encoding Flag-Snail1-WT or Flag-Snail1-3KR in the absence or presence of HA-A20. Cell lysates were immunoblotted. **e**, A20-depleted and control shGFP-expressing NMuMG cells were treated with TGF-β1 (5 ng/ml) for 24 h, followed by exposure to MG132 (10 μM) for 4 h and fractionated into cytoplasmic and nuclear extracts. Both extracts were immunoblotted with the indicated

antibodies. Expressions of tubulin and lamin were used as cytoplasmic and nuclear markers, respectively, and loading controls. **f**, A plasmid encoding Flag-Snail1-WT or Flag-Snail1-3KR was co-transfected into NMuMG cells with or without HA-A20 plasmid. Cell lysates were immunoprecipitated with anti-Flag antibody and subsequently immunoblotted. **g**, Chromatin immunoprecipitation analysis (ChIP) on NMuMG cells transfected with a plasmid encoding Flag-Snail1-WT or Flag-Snail1-3KR. Chromatin fragments were immunoprecipitated with anti-Flag antibody. PCR primers for E-cadherin promoter region were used to amplify the DNA isolated from the immunoprecipitated chromatin and input samples. The data in quantitative real-time PCR (lower panel) were statistically analyzed by a *t*-test and show the mean ± s.d. of *n*=3 independent experiments. \*\*\**P* < 0.01 compared to IgG control. n.s.; not significant. Images shown in this figure are representative of *n*=3 independent experiments. Expression of β-actin was used as a loading control for the immunoblot analysis except for **(e)**. Statistics source data for **(g)** are available in Supplementary Table 3. Unprocessed original scans of blots in **(a)** and **(c)**-**(f)** are in Supplementary Fig. 9.



**Supplementary Figure 7** A20 expression is induced by the Smad-independent noncanonical pathway upon TGF- $\beta$ 1 treatment. **a**, Gating strategy of CD44(+)/CD24(-) cancer cell populations in A20-depleted and control M4 (MCF10CA1a) cells. M4 cells were initially gated by FSC-A vs FSC-H for single cells and these separated cells were further gated by FSC-A vs SSC-A for the exclusion of debris. Live cells were finally gated by using fixable dye, APC-Cy7. **b**, After NMuMG cells were pre-treated with the TGF- $\beta$ 1 type I receptor inhibitor SB431542 (10  $\mu$ M) for 1 h, they were treated with TGF- $\beta$ 1 (5 ng/ml) for the indicated times. A20 expression and Smad2 phosphorylation were monitored by immunoblot analysis. **c**, **d**, NMuMG cells

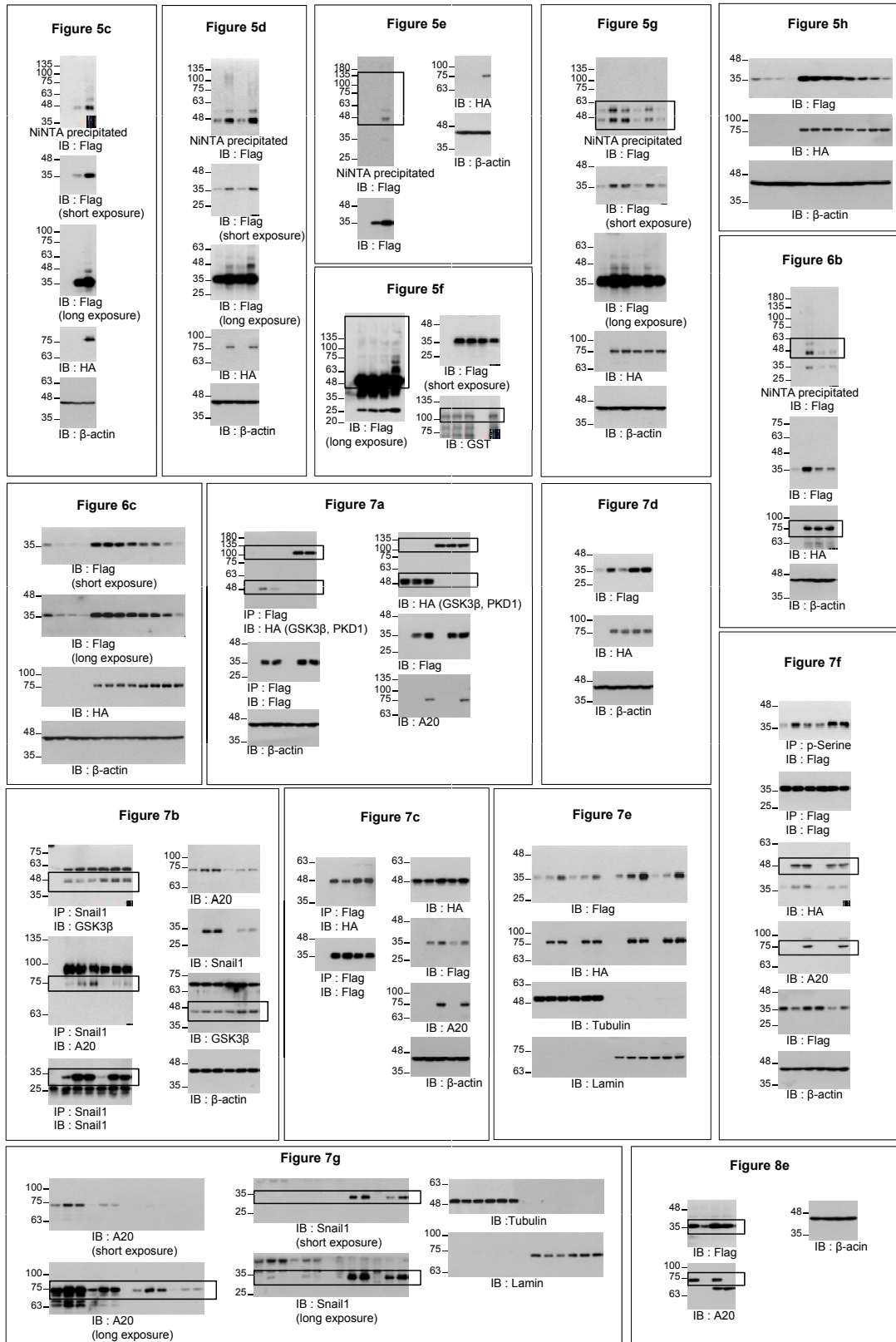
expressing Smad4-specific shRNAs or GFP-specific control shRNA were treated with TGF- $\beta$ 1 for the indicated times. A20 expression was analyzed by immunoblot (**c**) and quantitative real-time RT-PCR (**d**) analysis. In qRT-PCR analysis, expression of *Gapdh* mRNA was used for normalization. The data in (**d**) were statistically analyzed by a *t*-test and show the mean  $\pm$  s.d. of  $n=3$  independent experiments. All data of immunoblot analysis shown in this figure are representative of  $n=3$  independent experiments. Expression of  $\beta$ -actin was used as a loading control for the immunoblot analysis. Statistics source data for (**d**) are available in Supplementary Table 3. Unprocessed original scans of blots in (**b**) and (**c**) are in Supplementary Fig. 9.



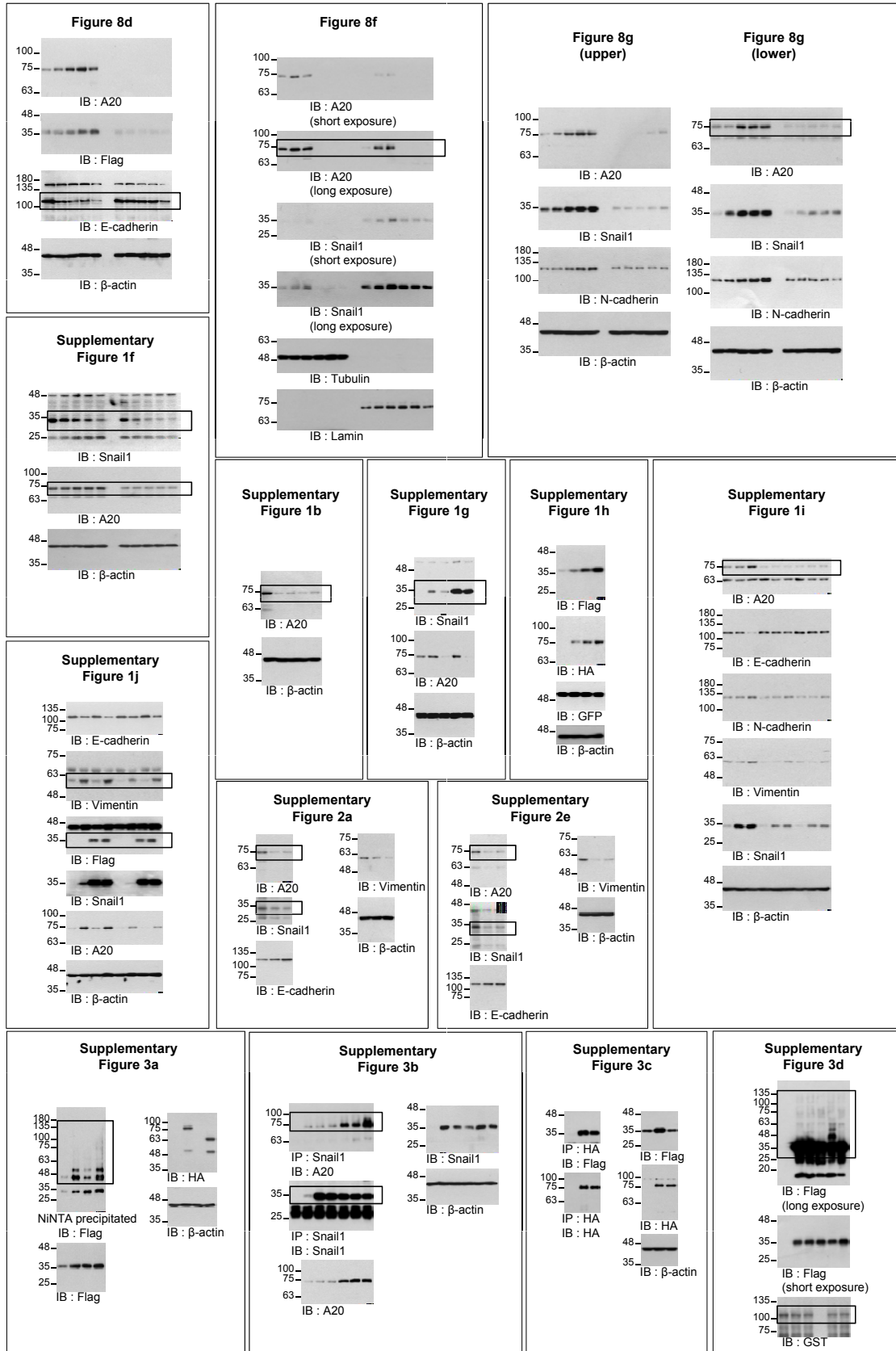
**Supplementary Figure 8** A20 expression is correlated with relapse-free survival of human breast cancer patients. **a**, Using Kaplan-Meier (KM) Plotter Tool (<http://kmplot.com/analysis>)<sup>66</sup>, the correlation between A20 expression and the relapse-free survival rates of breast cancer patients was analyzed in two independent public GEO datasets (left; GSE9195, right; GSE2603). *P* values were calculated using a log-rank test. HR = hazard ratio **b**, Proposed model demonstrating Snail1 stabilization by A20-mediated multi-monoubiquitination. In the absence of A20, Snail1 is phosphorylated by GSK3β at one of serine 107, 111, 115 and 119 residues and exported

from the nucleus to the cytoplasm. Additional phosphorylation occurs at one of the serine 96 and 100 residues by GSK3β in the cytoplasm. β-TrCP1 subsequently recognizes these Snail1 phosphorylations and builds a K48-linked polyubiquitin chain on Snail1, resulting in proteasomal degradation. In the presence of A20, Snail1 is monoubiquitinated by A20 at multiple sites of lysine 206, 234 and 235 residues in the nucleus. This multi-monoubiquitination inhibits the interaction between Snail1 and GSK3β. Thus, GSK3β-mediated Snail1 phosphorylation is decreased and Snail1 stability in the nucleus is increased, eventually promoting EMT and metastasis.

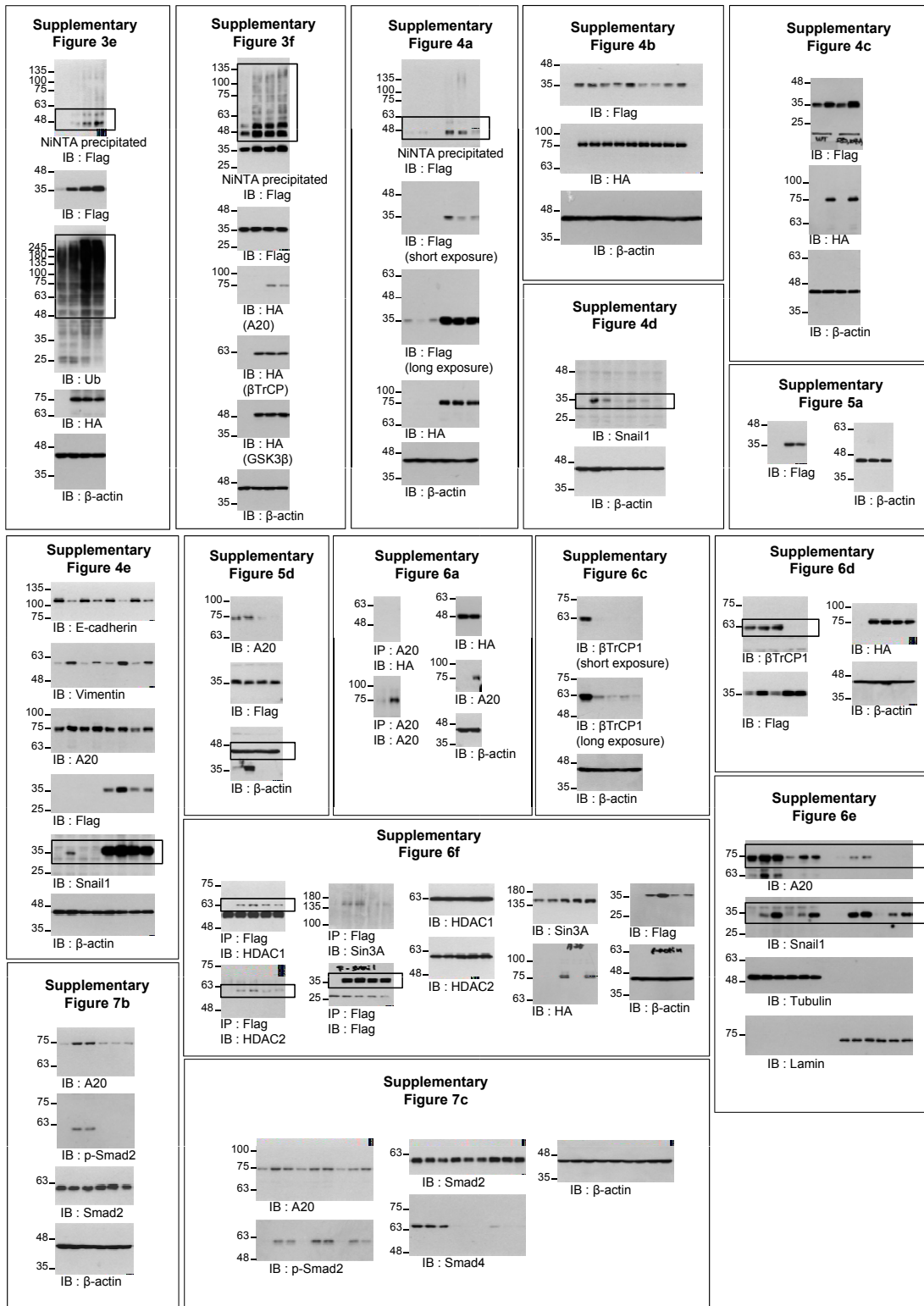




Supplementary Figure 9 Continued



Supplementary Figure 9 Continued



Supplementary Figure 9 Continued

## SUPPLEMENTARY INFORMATION

### Supplementary Table Legends

**Supplementary Table 1** Primary antibodies used in this study.

**Supplementary Table 2** Primer sequences and target sequences of shRNAs or siRNAs used.

**Supplementary Table 3** Statistics Source Data

## Life Sciences Reporting Summary

Nature Research wishes to improve the reproducibility of the work that we publish. This form is intended for publication with all accepted life science papers and provides structure for consistency and transparency in reporting. Every life science submission will use this form; some list items might not apply to an individual manuscript, but all fields must be completed for clarity.

For further information on the points included in this form, see [Reporting Life Sciences Research](#). For further information on Nature Research policies, including our [data availability policy](#), see [Authors & Referees](#) and the [Editorial Policy Checklist](#).

### ▶ Experimental design

#### 1. Sample size

Describe how sample size was determined.

No sample-size calculation was performed. Based on the literature, we chose the sample size routinely used in the field of molecular cell biology regarding reporter assays, quantitative real-time RT-PCR, cell invasion, migration, and proliferation assays (at least three independent experiments). All animal experiments to statistically analyze the results were performed with 6 mice per group.

For the analysis of A20 expression in tissue microarray (TMA), we prospectively collected tumor tissues from specimens of surgically dissected breast carcinoma at the Gangnam Severance Hospital, Yonsei University College of Medicine, Seoul, Korea, between January 1996 and December 2004. Among these samples, cases presenting an invasive focus by review of archival H&E-stained slides were used to construct tissue microarray (TMA) blocks. Two hundred fifty-six patients with invasive breast carcinoma were finally enrolled. To test a prognostic effect of A20 expression, sample size more than 200 cases is adequate to discriminate clinical outcome according to A20 expression.

#### 2. Data exclusions

Describe any data exclusions.

No data were excluded from the analysis.

#### 3. Replication

Describe whether the experimental findings were reliably reproduced.

For each experiment, all attempts at replication were successful.

#### 4. Randomization

Describe how samples/organisms/participants were allocated into experimental groups.

In animal experiments, mice were randomly allocated into each experimental group. However, a randomized sample selection in the experiment that explore A20 expression in human mammary carcinoma using TMA was not conducted due to its nature of retrospective study.

#### 5. Blinding

Describe whether the investigators were blinded to group allocation during data collection and/or analysis.

For animal data analysis, the observer was blinded to which animal of each group was being analyzed. The interpretation of immunohistochemical (IHC) stain was carried out blindly, without any information regarding clinical parameters or outcome.

Note: all studies involving animals and/or human research participants must disclose whether blinding and randomization were used.

## 6. Statistical parameters

For all figures and tables that use statistical methods, confirm that the following items are present in relevant figure legends (or in the Methods section if additional space is needed).

- n/a Confirmed
- The exact sample size ( $n$ ) for each experimental group/condition, given as a discrete number and unit of measurement (animals, litters, cultures, etc.)
  - A description of how samples were collected, noting whether measurements were taken from distinct samples or whether the same sample was measured repeatedly
  - A statement indicating how many times each experiment was replicated
  - The statistical test(s) used and whether they are one- or two-sided (note: only common tests should be described solely by name; more complex techniques should be described in the Methods section)
  - A description of any assumptions or corrections, such as an adjustment for multiple comparisons
  - The test results (e.g.  $P$  values) given as exact values whenever possible and with confidence intervals noted
  - A clear description of statistics including central tendency (e.g. median, mean) and variation (e.g. standard deviation, interquartile range)
  - Clearly defined error bars

See the web collection on [statistics for biologists](#) for further resources and guidance.

## ► Software

Policy information about [availability of computer code](#)

### 7. Software

Describe the software used to analyze the data in this study.

GraphPad Prism 5 Software and SPSS version 18

For manuscripts utilizing custom algorithms or software that are central to the paper but not yet described in the published literature, software must be made available to editors and reviewers upon request. We strongly encourage code deposition in a community repository (e.g. GitHub). [Nature Methods guidance for providing algorithms and software for publication](#) provides further information on this topic.

## ► Materials and reagents

Policy information about [availability of materials](#)

### 8. Materials availability

Indicate whether there are restrictions on availability of unique materials or if these materials are only available for distribution by a for-profit company.

All materials such as antibodies and reagents are available from for-profit companies. A20+/+ and A20-/- MEFs were provided by Geert van Loo, based on MTA. Our TMA slides of invasive breast cancer are available for further research such as exploring biomarkers and testing prognostic impact in breast cancer patients. They are not distributed by a for-profit company.

### 9. Antibodies

Describe the antibodies used and how they were validated for use in the system under study (i.e. assay and species).

Antibodies and their validation, including species and dilution ratio, were described in Supplementary Table 2 and the Online Methods (p2, p6).

### 10. Eukaryotic cell lines

a. State the source of each eukaryotic cell line used.

NMuMG, MCF10A and HEK293 cell lines were purchased from ATCC. A20+/+ and A20-/- MEFs were provided by Dr. Geert van Loo (Ghent University, Belgium). 4T1-Luc, MCF10AT, MCF10CA1h and MCF10CA1a cells were obtained from Dr. Seong-Jin Kim (Seoul National University, Korea). MCF7, T47D, MDA-MB-435, HS578T, SK-BR-3, BT-549, MDA-MB-231, ZR-75B and ZR-75-1 cells were provided by Dr. Seong-Jin Kim (Seoul National University, Korea). Human pancreatic cancer Panc-1 cells were kindly provided by Dr. Dong-Ki Lee (Sungkyunkwan University, Korea).

b. Describe the method of cell line authentication used.

The cell lines have not been authenticated in the present study.

c. Report whether the cell lines were tested for mycoplasma contamination.

All cell lines tested were negative for mycoplasma contamination.

d. If any of the cell lines used are listed in the database of commonly misidentified cell lines maintained by [ICLAC](#), provide a scientific rationale for their use.

No commonly misidentified cell lines were used.

## ► Animals and human research participants

---

Policy information about [studies involving animals](#); when reporting animal research, follow the [ARRIVE guidelines](#)

### 11. Description of research animals

Provide details on animals and/or animal-derived materials used in the study.

For tumorigenesis and metastasis analysis, 5-6 week old NOD/SCID female mice and 6 week old Balb/c female mice were used.

Policy information about [studies involving human research participants](#)

### 12. Description of human research participants

Describe the covariate-relevant population characteristics of the human research participants.

For retrospective transplantation studies with TMA slides, the need for informed consent was waived by the institutional review board of Gangnam Severance Hospital, Yonsei University, Seoul, Korea, in accordance with good clinical practice guidelines and the Declaration of Helsinki (3-2014-0239).

## Flow Cytometry Reporting Summary

Form fields will expand as needed. Please do not leave fields blank.

### ▶ Data presentation

For all flow cytometry data, confirm that:

- 1. The axis labels state the marker and fluorochrome used (e.g. CD4-FITC).
- 2. The axis scales are clearly visible. Include numbers along axes only for bottom left plot of group (a 'group' is an analysis of identical markers).
- 3. All plots are contour plots with outliers or pseudocolor plots.
- 4. A numerical value for number of cells or percentage (with statistics) is provided.

### ▶ Methodological details

- 5. Describe the sample preparation. 

We trypsinized the control or A20 depleted MCF10CA1a human breast cancer cells to dissociate single cell and thus we stained cell surface marker protein using fluorescence conjugated antibodies (FITC-anti-CD44, PerCP/Cy5.5-anti-CD24).
- 6. Identify the instrument used for data collection. 

We used FACSCanto II (BD Biosciences) for data collection.
- 7. Describe the software used to collect and analyze the flow cytometry data. 

We collected and analyzed the data using FlowJo 7.6.5 software.
- 8. Describe the abundance of the relevant cell populations within post-sort fractions. 

After gating, live cells were 98.7 %. CD24(-)/CD44(+) cells were 54.5 % in control M4 cells and 16.2 % in A20-depleted M4 cells when FACS analysis was completed.
- 9. Describe the gating strategy used. 

To gate samples for FACS analysis, cells were initially gated by FSC-A vs FSC-H for single cells and these separated cells were further gated by FSC-A vs SSC-A for the exclusion of debris. Live cells were finally gated by using fixable dye, APC-Cy7.

Tick this box to confirm that a figure exemplifying the gating strategy is provided in the Supplementary Information.